Discrete space charge affected field emission: Flat and hemisphere emitters

Kevin L. Jensen,[1,a)] Donald A. Shiffler,[2] Ian M. Rittersdorf,[3] Joel L. Lebowitz,[4] John R. Harris,[5] Y. Y. Lau,[6] John J. Petillo,[7] Wilkin Tang,[2] and John W. Luginsland[8]
[1]*Code 6854, Naval Research Laboratory, Washington, DC 20375, USA*
[2]*Air Force Research Laboratory, Kirtland AFB, New Mexico 87117, USA*
[3]*Code 6770, Naval Research Laboratory, Washington, DC 20375, USA*
[4]*Department of Mathematics and Department of Physics, Rutgers University, Piscataway, New Jersey 08854-8019, USA*
[5]*U.S. Navy Reserve, New Orleans, Louisiana 70143, USA*
[6]*Department of Nuclear Engineering and Radiological Sciences, University of Michigan, Ann Arbor, Michigan 48109, USA*
[7]*Leidos, Billerica, Massachusetts 01821, USA*
[8]*Physics and Electronics Directorate, AFOSR, Arlington, Virginia 22203, USA*

(Received 6 April 2015; accepted 5 May 2015; published online 19 May 2015)

Models of space-charge affected thermal-field emission from protrusions, able to incorporate the effects of both surface roughness and elongated field emitter structures in beam optics codes, are desirable but difficult. The models proposed here treat the meso-scale diode region separate from the micro-scale regions characteristic of the emission sites. The consequences of discrete emission events are given for both one-dimensional (sheets of charge) and three dimensional (rings of charge) models: in the former, results converge to steady state conditions found by theory (e.g., Rokhlenko *et al.* [J. Appl. Phys. **107**, 014904 (2010)]) but show oscillatory structure as they do. Surface roughness or geometric features are handled using a ring of charge model, from which the image charges are found and used to modify the apex field and emitted current. The roughness model is shown to have additional constraints related to the discrete nature of electron charge. The ability of a unit cell model to treat field emitter structures and incorporate surface roughness effects inside a beam optics code is assessed. © *2015 AIP Publishing LLC*.
[http://dx.doi.org/10.1063/1.4921186]

I. INTRODUCTION

Field emission sources generate high brightness electron beams that may meet the needs of particle accelerators, high power microwave (HPM) and x-ray sources, and vacuum electronic devices. The high current densities are a consequence of quantum mechanical tunneling through an emission barrier reduced in height and width by high electric fields at the surface. As a consequence, compared to other electron sources, such as photoemission and thermal emission, field emitter sources are much more profoundly affected by space charge near a single emission site,[1–3] space charge in the anode-cathode (AK) gap due to many emitters,[4–6] and field reductions at the apex associated with other close proximity emission structures otherwise known as "shielding" or "screening."[7–9]

The present analysis is the first part of a two part study undertaken to understand these interacting and degrading effects. The first and present study treats space charge and how it is affected by surface roughness or geometric features modeled as hemispheres. A distinction between the one-dimensional and three-dimensional models is the constraint imposed by the discrete nature of electron charge. The quantization of charge matters greatly in the treatment of emission from nano-scale emission sites and the behavior of space charge altered field emission near them: consequently, the discreteness model is introduced into the continuum 1D models as well to illuminate the correspondence and, more importantly, to emphasize that the nature of surface roughness affects how the discrete sheets of charge in the 1D model must be interpreted. The second part, reported separately, extends the roughness model to treat elongated wire-like emitters for the investigation of shielding effects on the emission process.[10,11] Taken together, such studies describe how space charge affects field (and therefore current) by means of field enhancement, shielding, changes to the tunneling barrier, and image charges associated with elongated structures, particularly long carbon fiber wire-like emitters presently undergoing characterization.[12] The models proposed are to be amenable to the shielding studies and therefore will not possess the rigor of more exact and simple 2D model systems[13,14] but will account for 3D effects. A method is proposed whereby the models can be integrated into beam optics codes, where field emission is difficult to treat because of the many orders of magnitude difference in length scales between emission site and electron gun,[15] and where displacement current effects would otherwise complicate the usage of a transit time model.[16] This is to be accomplished by means of a unit cell construction, the dimensions of which are dictated by the mean separation between adjacent emission structures. The space charge effects within the unit cell can be analyzed using a ring charge model developed herein to estimate the reduction of the field at the apex of an emitter due to previously emitted charge. The virtual anode of the

[a)]kevin.jensen@nrl.navy.mil

unit cell is close to the emission site so that the unit cell can be treated quasi-statically, thereby allowing the particle-in-cell (PIC) code to handle problems (such as transit time instabilities) that would otherwise be difficult or impossible to treat.

Regarding units and notation, q is the elementary unit charge such that the electron charge is $-q$, and it is the convention here to attach q to fields and potentials, and measure charge in units of q. Thus, $F = q\mathcal{E}$ is a force (units of [eV/nm]), and the image charge potential $V(x) = q\varphi(x) = \mu + \Phi - Fx - Q/x$ as well as the anode potential $V_a = q\varphi_a$ are in units of energy [eV]. The term $Q = q^2/16\pi\varepsilon_0 = 0.36$ eV nm is used in preference to ε_0. The usage of V and F instead of φ and $\mathcal{E}$ subtly modifies equations related to them, but the discussion will nevertheless speak of field and potential as is customary, although what is under discussion are instead forces and potential energies. Because of the units chosen (eV, fs, nm, and $q = 1$) a numerical equivalence exists between quantities expressed in [V] and [eV] as well as [GV/m] and [eV/nm]. Unless stated otherwise, conventions follow those used in Refs. 17 and 18.

Regarding terminology, the planar (1D) conditions will be contrasted repeatedly with the hemispherical (3D) conditions. It may be thought that rotationally symmetric emitters should properly be described as 2D. However, the introduction of adjacent emitters breaks the rotational symmetry. Therefore, whether or not a single emitter is under discussion, the circumstance will be referred to generically as 3D. Additionally, the convention will also be that ρ and σ refer to *number* densities rather than charge densities, so that the sign of the electron charge modifies conventional equations involving F, J, and ρ or σ (*e.g.*, Poisson's equation).

II. SPACE CHARGE AND FIELD EMISSION

The onset of space charge affected flow departs from the conventional Child-Langmuir limit when the emission mechanism is field emission in both one dimension[3,19–21] and multi dimensions.[6,14,22] The 1D analysis finds solutions that simultaneously satisfy Poisson's equation for electron density ρ and the Fowler Nordheim equation for current density J_{FN} (Eq. (A4)) using the assumption that current density (in [A/cm^2]) and number density are related via $J = -q\rho\langle v\rangle$ and that $\langle v\rangle \approx 0$ at the cathode surface. A more intuitive but less exact account is obtained using a transit time model,[17,23,24] which can be used to show that field emission can experience space charge limited (SCL) emission even though (as is common to assume) the potential energy does not pass through a maximum nor does the field at the surface vanish, but rather the *field strength* is limited, a point emphasized by van der Ziel.[25] It is therefore preferable here to speak of space charge affected field emission (SCAFE) (or "field-emitted vacuum space charge" (FEVSC) as Forbes[19] does), rather than SCL emission, to avoid activating intuitions which do not apply.

The dependency of SCAFE on surface field F can result in difficult to reconcile visualizations of what is occurring during the onset of space charge affected current flow. A common understanding of SCL current, leading to the Child Langmuir relation[6] (Eq. (B1)), is visualized as constant current density injected into the anode-cathode gap until the field at the surface of the emitter vanishes ($F \to 0$), but that would entail no field emission ($J_{FN} \to 0$). In 1D, the solution is to require F and $J(F)$ to simultaneously satisfy Poisson's equation and the Fowler Nordheim equation[1,19,21] (contrast with complimentary efforts to find consistent solutions using particle-in-cell codes[20] and simulation[26]), but the transition from a planar cathode to roughened surfaces (or an array of emitters) underscores the problem faced when attempting to reconcile steady state current with a microscopically rough or structured cathode, apart from the complexity already introduced by considering a small AK gap.[27,28] A possible solution uses a transit time model for separate regimes, the meso-scale regime governing discrete sheets of charge emitted from a planar cathode with a micro scale regime treating small surface structure or field emitter sites, with the later forming a unit cell within the former. The nature of discrete emission events, as in beam optics codes, differs in each case.

A. Transit time approximation

The transit time formalism[17,23,24] relates the field at the surface to the field across the AK gap separation in the absence of space charge ($F_o = V_a/D$), the temperature and field dependent current density at the surface $J(F, T)$ (Eq. (A1)), and the transit time (τ) measuring how long an electron takes to cross the AK gap by

$$F_o = F + \frac{q}{\varepsilon_0} N_\tau J(F)\tau(F), \tag{1}$$

where N_τ is a factor of order unity to bring the transit time model into line with the Child-Langmuir equation when the surface field vanishes (see discussion surrounding Eq. (9) of Ref. 17): it is 9/8 if the ballistic transit time $\tau(F) \to \tau_o$ is used. The temperature dependence in J is suppressed as T will be held constant.

In the absence of space charge in the AK gap, a solitary electron will experience a constant force $F_o = V_a/D$ acting on it that will accelerate it to the anode. The resulting "ballistic" transit time τ_o for that situation is well known from elementary kinematics to be

$$\tau_o = \sqrt{\frac{2mD}{F_o}}. \tag{2}$$

When a continuous and time-independent current density $J(F)$ for a surface field F is present, the transit time $\tau(F)$ has previously been shown to be[29]

$$\tau(F) = \frac{\sqrt{8mV_a}}{F}\left[1 + \left(1 + \frac{qJ(F)}{\varepsilon_o F^2}\sqrt{8mV_a}\right)^{1/2}\right]^{-1}. \tag{3}$$

Although the actual transit time τ exceeds the ballistic transit time τ_o, the difference is not substantial when $J(F)$ is small compared to $\varepsilon_0 F^2/(q\sqrt{8mV_a})$. The current density $J(F)$ cannot increase without limit: as more charge is injected into the AK gap, space charge forces suppress the surface F. In the extreme case when a single sheet is in the AK gap with

sufficient charge density to suppress F completely while the sheet is adjacent to the cathode, a second characteristic transit time results (see Eq. (9) below) and can be taken as an opposite limit.

Important features of sheet charge models appear in the works of Kishek and Lau[30] and Christenson *et al.*[31] The present approach summarizes key points. Let the position of the sheet in the AK gap be specified by $x = sD$, where $0 \le s \le 1$ is a scaled position. Further let the force between the sheet and the anode be denoted F_+, and that between the sheet and cathode be F_-. The relation $V_a = V(x) + (V_a - V(x))$ is then

$$F_o = F_- s + F_+(1-s). \tag{4}$$

The forces $F_\pm$ are related by Gauss's Law[32] $F_+ - F_- = \alpha F_o$, where $\sigma_o \equiv F_o\varepsilon_o/q^2 = F_o/(16\pi Q)$ and the sheet charge number density $\sigma \equiv \alpha\sigma_o$. Simultaneous solutions of these equations result in (compare Eqs. (16) and (17) of Ref. 17)

$$F_+ = (1+\alpha s)F_o, \tag{5}$$

$$F_- = (1-\alpha(1-s))F_o. \tag{6}$$

The force acting on the sheet of charge and causing it to accelerate is the average of the forces ahead of it and behind it (as can be determined by finding the force on a finite thickness uniform slab of charge and taking the thickness of it to zero). Therefore, the force equation from which the position is determined is given by

$$\frac{d^2 s}{dt^2} = \frac{F_+ + F_-}{2mD} = \frac{F_o}{mD}(2 - \alpha + 2\alpha s), \tag{7}$$

the structure of which is visible in Eq. (3a) of Ref. 30 for the two-sheet solution in the limit that the second sheet vanishes. This point will be revisited below in Eq. (17) when the position-dependence of the field produced by a sheet of charge in an AK gap is reconsidered. The solution of Eq. (7) for the transit time, defined by the equation $s(\tau) = 1$ (equivalently, $x(\tau) = D$) is

$$\tau(\alpha) = \tau_o \int_0^1 \frac{ds}{\sqrt{2s(2-\alpha(1-s))}}. \tag{8}$$

Consequently, $\tau(0) = \tau_o$ recovers the ballistic approximation. The opposite limit, $\tau(1)$ is the transit time for a sheet of charge with the maximum charge density $q\sigma_o$, and it is

$$\tau(1) = \sqrt{2}\tau_o \ln(1+\sqrt{2}) = 1.2465\tau(0). \tag{9}$$

Compare to Eq. (20) of Ref. 17 for an equivalent expression. Observe that Eqs. (3) and (9) are different, the former referring to continuous emission, and the latter to the emission of a single sheet of charge. It is seen that the single sheet transit time for $\alpha = 1$ is 25% larger than the ballistic transit time for $\alpha = 0$, that is, they do not differ greatly.

The first of two approximations that shall therefore be made herein is in relation to the transit time: the smaller ballistic transit time τ_o shall be used for all transit times encountered (usage of this lower limit will offset other approximations below, and it is accurate when the emission current is small). This is equivalent to taking a sheet of charge out of the AK gap (i.e., assuming it has reached the anode) when it has been in the gap for longer than τ_o. In effect, usage of the ballistic transit time underestimates the amount of charge in the AK gap. Its use results in the approximation

$$F_o \approx F + \frac{9q\tau_o(F)}{8\varepsilon_0}J(F), \tag{10}$$

where the "ballistic transit time" notation is now revised to be $\tau_o(F) \equiv \sqrt{2mD/F}$ such that $\tau_o(F)$ is evaluated using the surface field F rather than F_o. The value of F which satisfies Eq. (10) is close to that which is obtained through the simultaneous solution of Poisson's equation and the Fowler-Nordheim equation.[21]

As examples, consider a planar diode with an AK gap of $D = 10\ \mu$m and a cathode work function of $\Phi = 4.5$ eV (typical of metals and similar to carbon fibers). Let the field across the AK gap in the absence of space charge be $F_o = 6$ eV/nm. For room temperature conditions, $J \approx J_{FN}$ (Eq. (A4)) for the purposes of this example. Equation (10) then requires $F/F_o = 0.94117$, whereas the exact relation (compare Eq. (9) of Ref. 21)

$$\frac{J_{FN}(fF_o)}{J_{CL}(V_a, D)} = \frac{1}{9}\left(2 + (2-3f)\sqrt{1+3f}\right), \tag{11}$$

where $F_o = V_a/D$, $f = F/F_o$, and Eqs. (A4) and (B1) are used, demands $f = 0.93169$. The difference between $\tau(F)$ and τ_o is approximately 1%. The transit time approach is therefore reasonable. Changing F_o to 10 eV/nm, Eq. (10) then requires $f = 0.68613$, whereas the exact relation demands $f = 0.67488$. The difference between $\tau(F)$ and τ_o is now approximately 3%. The relaxation time approach remains reasonable even when field emission is high. The results of this exercise demonstrates that current density, not transit time, is the primary determinant of F for field emission, as a consequence of the very strong variation of $J(F)$ with F—this allows the consideration of field emission to be treated differently than other emission mechanisms, where the transit time is much more influential, and enables an opportunity in that a reasonable and easily calculated transit time $\tau_o(F)$ may be used, simplifying the quantification of space charge effects on the emission barrier.

The use of the surface field F in the evaluation of the ballistic transit time $\tau_o(F)$ rather than the larger field F_o offsets some of the underestimation of surface field reduction due to space charge in the AK gap. A more important offset will be due to a second approximation that shall be made, which has the same effect as overestimating the effect of space charge in the AK gap, and concerns the usage of Eq. (19) below. The adequacy of the two approximations will be assessed in Sec. III.

B. Surface roughness

Simulating the transition from field emission dominated current density to space charge affected flow using PIC codes[20,33] is desirable given PIC's ability to track particle

motion and monitor the duration of time charge remains in the AK gap for finite-sized emission regions (similar comments apply to molecular dynamics (MD) simulations[26]). For uniform and extended planar emitters (e.g., thermionic cathodes) findings comport well with analytical methods,[34] but field emission from small active regions significantly burdens simulation. In particular, surface roughness is problematic for PIC.[18]

In the 1D model, there is liberty in how many discrete sheets $n = \tau/\Delta t$ are used to approximate continuum emission and so there is freedom in the choice of Δt. The presence of surface roughness and its associated field enhancement change matters, but because the effects of surface roughness are only dominant near the cathode, components of the 1D formalism can be profitably retained. The differences between the 1D and 3D models are then related to local field enhancement and the possibility of shielding due to geometry.

Surface roughness can be modeled as a speckling of a plane with small hemispherical bumps ("bosses") of radius a. Field variation over a bump is governed by $F(\theta) = 3F_o\cos(\theta)$, where θ is the polar angle (see discussion surrounding Eq. (32) below). Consequently, the apex field is $F_{tip} = 3F_o = 3V_a/D$ ($\beta = 3$). Let the current from a hemisphere be designated I_{boss}, which depends on the current density $J(F_{tip})$ and the "notional emission area" factor $g(F)$ (a measure of the fraction of the hemispherical surface that is emitting[18,35] and given by Eq. (34) which scales with the actual emission area). For $F_o = 2.5$ eV/nm, then $g(3F_o) = 0.083882$. Assume that the hemispheres are spaced sufficiently widely apart so that they do not shield each other appreciably: a "tip-to-tip" separation of $d_{tt} = 5a$ is adequate, with hemispheres being on a square grid, larger than but comparable to the "optimal" prescription (Ref. 9, and references therein). The impact of shielding is related to the separation between emission sites, and therefore dictates the dimensions of the unit cell model treating a single site.

The average current density is $J_o = I_{boss}(V_a)/d_{tt}^2$, with all of the current originating from the hemispheres as the field is too weak at the surface between the hemispheres for appreciable emission (e.g., $J_{FN}(F_o)d_{tt}^2/I_{boss}(V_a) \approx 4.7\times10^{-7}$ for $F_o = 2.5$ eV/nm). Unlike the 1D model, in the limit of very small emission currents, the emission must be treated as a series of discrete emission events, rather than a continuous flow of charge. Thus, a characteristic time $\Delta t = q/I_{boss}(V_a)$ is the average time between emission events and is constrained because the electron charge is discrete. After the electrons move several d_{tt} away from the surface, the lattice of emitted charge can again be modeled as a "sheet of charge."

Using $J_o = I_{boss}(V_a)/d_{tt}^2$ in place of J_{FN} in Eq. (10), with $V_a = F_oD$, $F_o = 2.5$ eV/nm and $D = 10\,\mu$m results in $F = 0.93137F_o$ being the self-consistent field. Such a reduction modifies the current per hemisphere to 46% of the space charge free condition. However, $\Delta t = 1.62\tau_o(F_o)$ so that for a nontrivial fraction of the time, no charge is in the gap when the current is (on average) space charge affected. The problem therefore is affected by similar physics to that described by Zhu and Ang[36] who investigate the relation of space charge limited current to the Coulomb blockade regime. Observing that the emission of charge is a statistical event for which Δt is the mean time between emission events deepens the mystery: there will be times where more charge is in the gap than permitted by Eq. (10), and times where less is, and so the emission will be *noisy*. Further, the role of space charge in the discrete-emission limit therefore differs subtly but importantly from a conventional intuition regarding the role of space charge in the continuous-emission limit: in the later, charge in the AK gap reduces the *quantity* of emitted current in a direct, immediate, and continuous way, while in the former, the presence of charge in the AK gap reduces the *probability* of subsequent emission events on average but does not prevent the presence of quantities of charge in the gap that are above-average or below-average for a given surface field. Finally, emission will also occur off-axis, and that will introduce transverse velocity effects and transit time changes, complications with no analog in the 1D formulation. Hence, the 3D models based on hemispheres entail additional physics.

Several conclusions follow. First, steady and continuous emission as implied by the transit time approach gives way to the complexity of fluctuating discrete emission events governed by the magnitude of unit electron charge that on average give rise to J_o. Second, in the low current limit, the role played by space charge is to change the *mean time between the emission events* for each hemisphere. Third, when the hemispheres are modified so that they are either in more dense arrays or elongated in shape, their susceptibility to shielding effects from adjacent structures may magnify, making the analysis more complex.

In Sec. III, the consideration of the planar or 1D problem as random emission events and the subsequent changes in emission that result is given and focuses on fluctuations caused by meso-scale sheets of charge density. In Sec. IV, roughness is introduced and its impact on emission by changes to the image charge, the relation between the trajectory arc in the AK gap and the transit time, and the effect on emission probability that results is related to the fluctuations caused by micro-scale emission events that are localized to an emission site associated with a geometric feature. The nature of emission probability, intrinsic to both, is related to Poisson statistics.

C. Poisson statistics

In the absence of space charge effects, electron emission events are generally considered to be independent and emitted at random times. The number emitted per unit time is given by a Poisson distribution[37–40] and results in a shot noise spectrum.[41,42] That is, the probability of emission in any (infinitesimally small) time interval dt is λdt, while the probability of k emissions during a time interval of duration t is

$$p_k(t) = \frac{(\lambda t)^k}{k!}e^{-\lambda t}, \tag{12}$$

for $k = 0, 1, 2, \ldots$ In particular, the probability of no emission, $k = 0$, is $p_0(t) = e^{-\lambda t}$, while the probably of having an

emission in the (infinitesimal) time interval dt after waiting a time t is just $e^{-\lambda t}\lambda dt$, where $\lambda = 1/\Delta t$ is the average time between emissions. In the 1D models, the events correspond to the emission of a sheet of charge with charge density $q\sigma = J\Delta t$. In the 3D models, the events correspond to the emission of a bunch of charge with a total charge $I_{boss}\Delta t$. The interpretation of λ will change between the sheet and bunch models, but to simplify the discussion, both will be referred to as "events," and the average number of events per unit time is the average current (3D) or current density (1D).

If the AK gap is large and the emission strong, then the number of events per unit time should be significant. A bump of radius 5 nm with an apex field of $3F_o = 7.5$ eV/nm will have a micro-scale current of $I_{boss} = 6.3\,\mu$A, so that an electron is emitted every $\Delta t = q/I_{boss} \approx 25$ fs on average. For an AK gap of $D = 10\,\mu$m, a transit time of $\sqrt{2mD/F_o} \approx 200$ fs results, suggesting that there are about 8 events on average in the gap. The meso-scale sheet charge density is then determined by the tip-to-tip spacing d_{tt} by $q\sigma = I_{boss}\Delta t/d_{tt}^2$. Equation (12) then specifies the probability that in fact there are k sheets instead, and is shown in Figure 1.

Consequently, it is evident that some emission events can be very closely spaced to each other. If the probability of an event *not* occurring in a time t is $p_0(t) = \exp(-\lambda t)$, then for N emission events, each event corresponding to an individual Δt_j for how long after the previous event it occurred, can be grouped into bins. Doing so results in Figure 2, although N and λ are changed to $N = 4096$ and $\lambda = 1/(32$ fs) to make the behavior of interest more apparent. It is clear that many events occur for Δt_j a fraction of the average Δt.

The previous discussion treats λ as unaffected by prior emission events, but field emission is inordinately sensitive to space charge forces. The reduction of the surface field by a small amount greatly affects $J_{FN}(F)/J_{FN}(F_o)$. For standard metal parameters, the sensitivity is shown in Figure 3 for the cases of 1% ($F/F_o = 0.99$) and 5% ($F/F_o = 0.95$). As a consequence of that sensitivity, structure is imposed on $F(t)$.

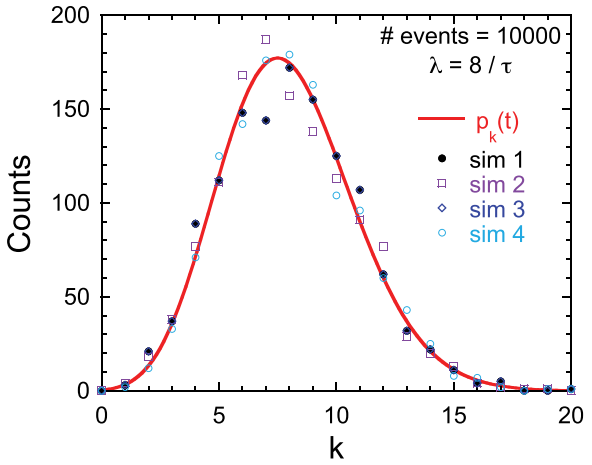

FIG. 1. Distribution of events in the AK gap as per Eq. (12) (red line) in four simulations. Events randomly occur until the time separation between first and last exceeds the transit time $\tau = 200$ fs. Instances where there are *no* events in the AK gap occur, as do instances where there are multiples of the average number of 8.

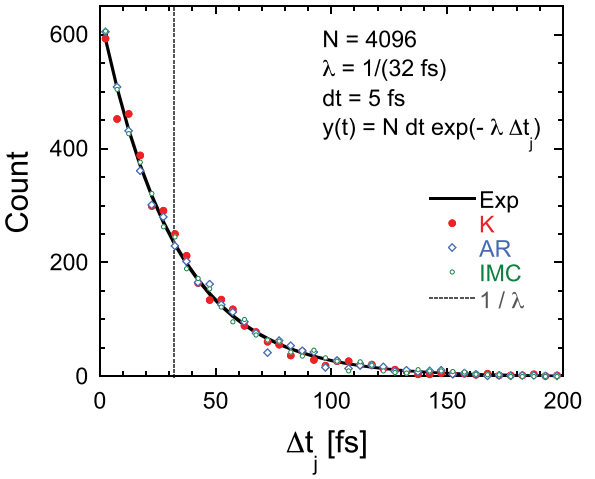

FIG. 2. Comparison of the number of Δt_j ("count") falling into bins of size $10/64\lambda$ using Eq. (23) (K), compared to an acceptance/rejection algorithm (AR) and a binned Monte Carlo method (IMC) described in Appendix C. N is the total number of Δt_j. A curve $Ndte^{-\lambda\Delta t_j}$ is overlaid (Exp). The dashed vertical line is $\Delta t = 1/\lambda$.

III. DISCRETE EMISSION FROM A PLANE

A. Sheet charge models

In a continuum model, current and number density ρ are related by $J = -q\rho v$. In steady state, current is without fluctuation (field emission requires the maintenance of substantial fields *at the surface*, so that return trajectories as seen in Ref. 34 do not modify the analysis). On the other hand, if sheets of varying charge density are randomly emitted, then fluctuations in the occurrence of emission events are a natural and expected consequence. Sheet-like emission models reveal time dependent behavior from planar thermionic emission structures,[37] and the accuracy of sheet models has been remarked upon for the simulation of thermionic cathodes.[43]

The average number of events per unit time is λ. If the emission times are distributed, the variance is minimized by taking $\lambda \to \infty$ such that the continuous emission model[21] is recovered. In nature, however, the charge emitted is fixed by the charge of the electron, and that affects the three dimensional models, but for one dimension where sheets of charge

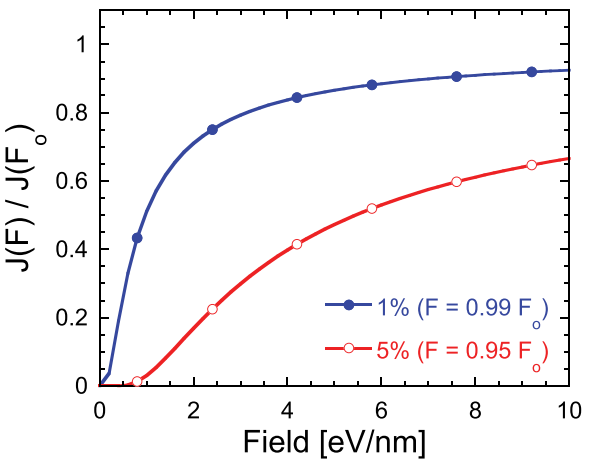

FIG. 3. Ratio of the current density for a small reduction in field ($F < F_o$) for standard metal parameters ($\mu = 7$ eV and $\Phi = 4.5$ eV).

density $q\sigma$ are emitted, there remains some freedom in the choice of both σ and λ.

The surface field $F(t)$ will depend on the number of sheets in the AK gap, and on the charge density $q\sigma$ per sheet. The simplest case is a sheet charge density of $q\sigma_o = \varepsilon_0 F_o$ so that there is at most one sheet in the AK gap, that is $F(t) = F_o$ if no sheet was emitted in the time interval $[t-\tau, t]$ so $\lambda(t) = \lambda_o$ while $\lambda(t) = 0$ if there was an emission event in that interval. The single sheet transit time is known exactly.[17] The situation is much more complicated when k–sheets ($k > 1$) are emitted. There are alternative ways of modeling the situation: for example, $\sigma(t)$ can depend on $F(t)$ with λ held fixed, or the emission can be taken to be periodic. Of the various so-called toy models that are possible, the ones here are based on the transit time τ associated with field emission and the nature of the fields produced by a sheet of charge density $q\sigma$. As the sheet accelerates across the anode-cathode gap, its presence reduces the field at the surface of the cathode until such time as the sheet is absorbed by the anode. The degree to which the jth sheet of n sheets reduces the surface field depends on its charge density $q\sigma_j$ but also, as shall be shown, its position x_j as well.

The cumulative effect of the n sheets invokes methods behind the two-sheet model of Kishek and Lau[30] and the many sheet model leading to Eqs. (7) and (A3) of Christenson *et al.*[31] Consider first the field reduction at the surface of the cathode due to the presence of one sheet of charge in the AK gap. The surface term F is determined as follows. Poisson's equation, using the conventions described in Section I (in particular, $Q = q^2/(16\pi\varepsilon_0)$), is

$$\frac{d^2}{dx^2}V(x) = 16\pi Q\rho(x), \tag{13}$$

where the negative charge of the electron ($-q$) and the usage of a number density off-sets the negative sign conventionally present, and where the number charge density $\rho(x) = \sigma\delta(x - \bar{x}(t))$, where $\bar{x}(t)$ is the trajectory of the sheet. The general solution is the sum of the particular solution $V \to V_p$ in Eq. (13) and the homogeneous solution V_h determined from $d^2V_h(x)/dx^2 = 0$. The boundary conditions are $V_h(0) = 0$ and $V_h(D) = V_a$ and $V_p(0) = V_p(D) = 0$. The potential energy $V(x)$ is the sum, or $V(x) = V_p(x) + V_h(x)$. $V_h(x)$ is given by $V_h(x) = xV_a/D$. $V_p(x)$ invokes Gauss's law[32] and relates the sheet charge density to the difference of the forces on each side of the sheet or

$$\frac{V_p(x) - V_p(0)}{x} - \frac{V_p(D) - V_p(x)}{D - x} = 16\pi Q\sigma, \tag{14}$$

which, in light of the boundary conditions and introducing the notation $\sigma/(16\pi Q) \equiv \alpha F_o$, becomes

$$\frac{V_p(x)}{D} + \frac{V_p(x)}{D - x} = \alpha F_o. \tag{15}$$

The general solution is then

$$V(x) = xF_o - \alpha F_o \frac{x}{D}(D - x). \tag{16}$$

The force F at the surface due to a sheet of charge in the AK gap at position x is therefore governed by ratio of the potential energy at the location of the sheet $V(x)$ with the distance to the sheet x or

$$F = F_o - \alpha F_o\left(1 - \frac{x}{D}\right). \tag{17}$$

Observe that this is the force *acting on the sheet*; the force on a particle external to the plane of the sheet satisfies a similar equation but with $\alpha \to \alpha/2$.

For a sheet in the AK gap, the impact of the sheet is greater the closer it is to the cathode surface (in contrast to a sheet of charge in free space for which the field created by it is independent of distance). When there are n sheets in the gap, then, by superposition,

$$F = F_o - 16\pi Q\sum\nolimits_{j=1}^{n}\sigma_j\left(1 - \frac{x_j}{D}\right), \tag{18}$$

$$= F_o\left\{1 - \sum\nolimits_{j=1}^{n}\alpha_j(1 - s_j)\right\}, \tag{19}$$

a result equivalent to Eq. (A5) of Ref. 31 when the observation point is the surface of the cathode. The second approximation to be proposed concerns how this result is handled: evaluating Eq. (19) is complex because the positions of the sheets x_j (equivalently, s_j) are required, and they are not in general available until the solution to Eq. (19) is available. Stated another way, finding F necessitates finding both σ_j and x_j, but x_j is dependent on the field that existed on the surface at the time of emission, and the position ("trajectory") of the sheet as it is accelerated in a time-dependent field, both of which are unknown. A simple solution is therefore not forthcoming for analytical methods, although intensive methods such as those of Caflisch and Rosin[34] can make headway. A simple solution, though, is highly desirable given its utility in guiding approximations when surface roughness is present, and particularly for modeling elongated or wire-like structures as are under consideration.[12,18]

The proposed simple, or qualitative, solution is as follows. The reduction of the surface field δF is given by the second term of Eq. (19). Contrast this to a model which does not include the position dependence, or $\delta F_o = \sum_{j=1}^{n'}\alpha_j$, but where $n' < n$ is the smaller number of sheets in the gap because the sheets are allowed to stay in the gap only for a time τ_o. For purposes of a representative model, a single sheet traveling ballistically will follow $x(t) = D(t/\tau)^2$, and so $x_j/D \sim (t_j/\tau)^2 = (j/n)^2$. Next, because the current density $J(F)$ is exponentially dependent on $1/F$, then σ_j will depend on the sum of the sheets emitted prior to the j^{th} sheet: thus, let $\sigma_j \sim \sigma_o \exp(-a(\tau - t_j)/\tau)$, where a is a parameter that governs how rapidly the charge density declines for subsequently emitted sheets. The questions are then, what error is expected from the neglect of the position dependence in Eq. (19) in the single sheet limit ($a \to \infty$) and in the steady state limit ($a \to 0$)?

For the single sheet limit, $a \gg 1$ corresponds to the actual transit time approaching the value given by Eq. (9) (the charge density of the first sheet dominates the others),

and because the difference between $\tau(F)$ and $\tau_o(F)$ is only 25%, let $n = 5n'/4$. Then, if the emission events are uniformly spaced, the ratio of the actual field reduction δF to δF_o behaves as

$$\frac{\delta F}{\delta F_o} \sim \frac{\sum_{j=1}^{n} \left(n^2 - j^2\right) e^{-a(n-j)/n}}{\sum_{j=1}^{4n/5} e^{-a(n-j)/n}}. \tag{20}$$

The behavior of Eq. (20) for various n (chosen so that $n' = 4n/5$ is integer) are shown in Figure 4.

For the steady state limit, $a \to 0$ entails the α_j become equal, and so

$$\lim_{a\to 0} \frac{\delta F}{\delta F_o} = \frac{5}{6}\left(1 - \frac{3}{4n} - \frac{1}{n^2}\right), \tag{21}$$

which converges to 0.8333 for $n \to \infty$ and is 0.7 for $n = 5$.

In both cases, it is seen that the approximations (henceforth referred to as the $s - \tau$ approximation), first of neglecting the s_j term in δF and second of using the ballistic transit time τ_o as the transit time, are sufficient to enable a reasonable qualitative model from which behavior can be inferred, although a loss of a quantitatively predictive capability is expected. When a surface roughness model is introduced, the circumstances improve, as near the cathode surface is where a "unit cell model" of surface roughness is sought, and it is there that the $s - \tau$ model performs well.

The $s - \tau$ approximation is equivalent to letting the field at the surface of the cathode be governed by

$$F_{j+1} = F_j - \frac{q\Delta t}{\varepsilon_0} J(F_j). \tag{22}$$

Immediately after emission starts, the surface field begins to drop in increments which causes the current density to decline until sheets begin to be absorbed at the anode and no longer contribute to the surface field reduction. The assumption frees the model from the need to monitor and update the location of the sheets: only the duration of time they remain in the AK gap matters. One therefore expects the initial oscillations (due to either uniformly or randomly emitted events) to damp over time, converging on a result comparable to the continuum limit of Eq. (11). The initial oscillations, which will be shown subsequently, is reflected in the more accurate numerical simulations of Feng and Verboncoeur (see Figure 5 of Ref. 20), and more recently in the work of Torfason *et al.*,[26] whose Figure 4 in the case of a large emission area is anticipated by the results of the simple models below, as shall be shown.

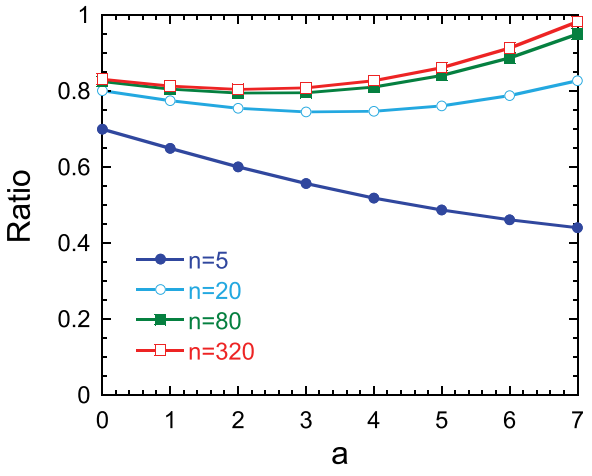

FIG. 4. The ratio given by Eq. (19) as a increases for various n. As a and n become large, the single sheet model of Eq. (9) is approximated, and so the ratio should approach unity.

Let the sheets be labeled according to their position with respect to the surface: if there are n sheets in the AK gap, then the sheet n is closest to the anode and the $i = 1$ sheet is just off the cathode surface. The indexing of Δt differs from t_i: Δt_1 refers to the first sheet *emitted* and is closest to the anode. Consequently, the time steps are calculated according to $t_{i+1} = t_i + \Delta t_{n+1-i}$. Only those sheets for which $t_i \le \tau_o$ are allowed to contribute to the field reduction at the surface, a restatement of the approximation to use the ballistic transit time τ_o over the actual transit time $\tau(F)$, which in steady state will underestimate the field reduction by the small amount $J(F)(\tau(F) - \tau_o)/\varepsilon_0$. The three models (labeled M1 trough M3), therefore, refer to three cases of increasing complexity in the treatment of Δt_j and the emission probability in the context of the $s - \tau$ approximation.

M1: For uniform emission events, $\Delta t_j = \Delta t$ for all sheets: the variation in the sheets is therefore contained in the changing sheet charge density $\sigma_j = J(F_j)\Delta t$. There are n sheets in the gap at any time and $n\Delta t = \tau_o$.

M2: If the emission of a sheet of charge is a random event, then the time a sheet of charge is emitted after the prior one, or Δt_i, is found by

$$\Delta t_i = -\ln(r_i)\Delta t, \tag{23}$$

where r_i is a uniformly distributed random number in the range between 0 and 1, and Δt is the mean value. The basis for this equation is given in Appendix C.

M3: The probability of emission is a random event, governed by the ratio of the current density to the maximum current density, and the emission of a sheet is randomly dictated using a Monte Carlo (MC) algorithm. The position of the sheets can be tracked so that Eq. (19) can be used.

For the second model, the Δt_j that result as a consequence of Eq. (23) have been shown in Figure 2 as the line labeled "K," compared to a standard method of choosing Δt_j using acceptance/rejection techniques labeled "A/R" (a third method, based on the last "alternate" method of Appendix C, is labeled "IMC"). The agreement is good. Observe that some values of Δt_j can be comparable to the transit time τ_o. The third, or Monte Carlo, model is significantly different than the previous two, and will be discussed separately. It can either mimic the $s - \tau$ approximation or keep the position-dependence of Eq. (19), and so it serves to quantify the cost of the $s - \tau$ assumptions.

All findings shall be compared to the analysis of Rokhlenko *et al.*, which determined that the steady state

self-consistent field emission current density is (Eq. (9) of Ref. 21)

$$\frac{J(F)}{J_{CL}(V_a,D)} \equiv j = \frac{1}{9}\left(2 + (2-3f)\sqrt{1+3f}\right), \tag{24}$$

where $f = FD/V_a$, $J(F) \to J_{FN}(F)$ is Eq. (A4), and J_{CL} is Eq. (B1). The values of j and f are then found numerically (bisection followed by a correction using finite difference methods).

B. Results: Models 1 and 2

For metal parameters ($\mu = 7$ eV, $\Phi = 4.5$ eV) at low temperatures ($J(F) \approx J_{FN}(F)$), the solution to Eq. (24) is satisfied by $f = 0.86005$ and $j = 0.18252$ if $F_o = 7$ eV/nm and $D = 10\,\mu$m. These values represent the expected asymptotic limits of the time-dependent analyses. Consider two choices of Δt for the time-dependent analysis. If $\tau_o/\Delta t = n = 100$, then Figure 5 results. By contrast, if $\tau_o/\Delta t = 1000$, then Figure 6 results. In these figures, the smooth curves (light blue for field, purple for current) represent M1 results, and the jagged curves (dark blue for field, red for current) represent the M2 results. The nature of the oscillations are comparable to the numerical results in Figure 5(b) of Feng and Verboncoeur[20] or Torfason *et al.*[26] Significantly, such oscillations are seen in the analytic one dimensional treatment of Rokhlenko and Lebowitz[44] (their Figure 1): although the sharp cusps evident in the present work are softened by comparison, the damped oscillations are evident. Thus, when $n = \tau_o/\Delta t$ is large then M2 better approximates M1. The more important point, however, is that if the value of n and therefore Δt is limited by an independent requirement (such as the discrete nature of electron charge and the spacing of emission sites), then progressively small values of n result in progressively noisier behavior in $J[F(t)]$, and will have consequences with how noise is introduced into a simulation.

Representative evaluations make the point. For $F_o = 7$ eV/nm, $J_{FN}(F_o) = 2.374 \times 10^7$ A/cm^2. For the choice $\Delta t = 1.27$ fs, the sheet charge density is 1 electron per

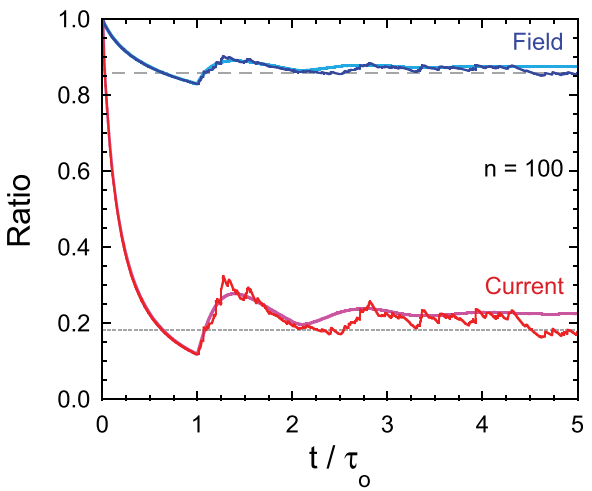

FIG. 5. Evolution of $F(t)$ (Eq. (22)) and $J[F(t)]$ for $F_o = 7$ eV/nm and $D = 10\,\mu$m for $\Delta t = \tau_o/100$ and Δt_j from Eq. (23). Gray lines determined from Eq. (11).

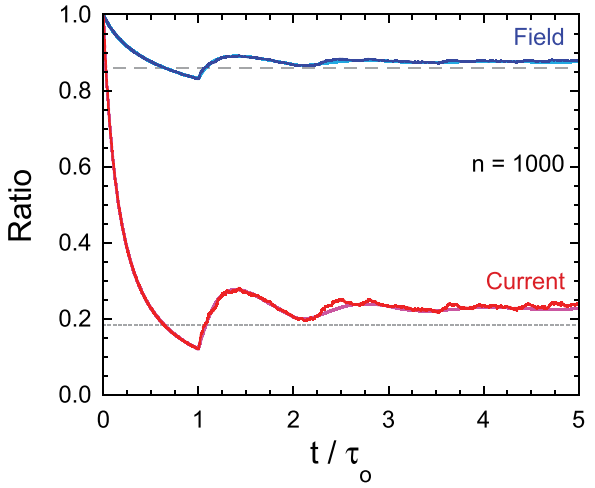

FIG. 6. Same as Figure 5 but for $\Delta t = \tau_o/1000$ and Δt_j from Eq. (23).

(23 nm)^2. If shielding effects from adjacent geometric structures approximating surface roughness affect emission and cause emission events to be correlated from one site to the next, then smaller n values may be more physical. The hemispherical bump model is intended to address this, as the introduction of roughness sets a length scale that allows a consideration of physical processes to affect the time scale, but it will require a consideration of how the planar image charge is modified in the vicinity of a curved surface and the contribution of emitted charge in suppressing the surface field.

C. Results: Model 3

Let the probability that an electron is *not* emitted in a time t be $p = \exp(-\lambda t)$. A sequence of δt_j such that $t_j = \sum_{k=1}^{j} \delta t_k$ entails that the probability $P(t_j)$ that an electron will be emitted at t_j is

$$P(t_j) = p(\delta t_1)\ldots p(\delta t_{j-1})(1 - p(\delta t_j)) \tag{25}$$

or the product of probabilities that the electron is *not* emitted (p) in the $j-1$ steps before t_j but emitted ($1-p$) on the last step δt_j. If the time steps are equally spaced,

$$\sum_{j=1}^{\infty} P(t_j) = \sum_{j=1}^{\infty} e^{-(j-1)\lambda\delta t}(1 - e^{-\lambda\delta t}) = 1. \tag{26}$$

$P(t)$ is representable as the number of emission events to the number of emission attempts. For emission in sheets, the accumulation of sheets constitutes the injection of charge into the anode-cathode gap (a model applied to thermal emission by Birdsall and Bridges[37]). The number of electrons emitted per unit area is $J(F)\Delta t/q$, and the number of attempts is $J_{max}\Delta t/q$. In terms of the supply function $f(E)$ (in a notation following Ref. 45)

$$\frac{J(F)}{J_{max}} = \frac{\int_0^\infty D(E)f(E)dE}{\int_0^\infty f(E)dE} \equiv R(F), \tag{27}$$

where $E = E_x$ is the normal energy (or energy into the barrier). For metals, $J_{max} = (3/16)q\rho(\hbar k_F/m) = mq\mu^2/(4\pi^2\hbar^3)$

in the $T \to 0$ K limit, where $\rho = k_F^3/3\pi^2$ is the number density ρ of the zero-temperature electron gas. Letting $J = J_{FN}$ and using Eq. (A4), gives the ratio in Eq. (27), defined as $R(F)$, as

$$R(F) = \frac{\hbar^2 F^{2-\nu}}{4m\Phi\mu^2 t_o^2}\left(\frac{\Phi^2 e^6}{4Q}\right)^{\nu} \exp\left(-\frac{B\Phi^{3/2}}{F}\right). \quad (28)$$

The probability that an electron is emitted in time t is $\{1 -$ (the probability that it is not)$\}$, or

$$1 - \exp\{-\lambda(F)t\} = R(F). \quad (29)$$

Let the ratio of the time step δt for the Monte Carlo simulation to the characteristic time Δt defined by the current density be $n = \Delta t/\delta t$. The probability that an emission event does not occur in a time t_j is

$$p(t_j) = \left\{\prod_{l=0}^{j}(1 - R_j)\right\}^{1/n}, \quad (30)$$

where the shorthand $R_j \equiv R(F_j)$ is used. When sheets of charge are in the AK gap, then in the $s - \tau$ approximation

$$F_j = F_o - \frac{q\Delta t}{\varepsilon_0}\sum_{l=0}^{j-1} J(F_l), \quad (31)$$

and because $(1 - R_j)^{1/n} < (1 - R_0)^{1/n}$ it is seen that the effect of space charge is to reduce the probability $p(t)$ by a small amount over the transit time of the previously emitted sheet across the AK gap. Thus, space charge reduces the average current even when the characteristic time Δt is larger than the transit time τ.

A code to model the emission of uniform sheets of electrons based on the quantum mechanical probability of emission while also keeping track of the electron sheets as they transit the diode gap using the Monte Carlo approach was developed. The acceleration that each sheet experiences is not constant, but rather a function of time due to the shielding of the vacuum field by the space charge between each sheet and the anode. The initial velocity of the sheet is assumed to be negligible (zero). Charge overtaking (in which one sheet moves ahead of a previously emitted sheet) of these sheets is observed in these simulations. The simulation begins with the initial sheet of charge being emitted at time $t = 0$ and then steps forward by a specified time step, δt. The positions of the sheets of charge are then advanced according to the accelerating field that they experience, given by F_j. Any sheets passing the location of the anode are considered collected and removed from the simulation.

Following the kinematic update to each sheet's position, a check is made to see if the cathode emits another sheet of charge. The emission event at the cathode is determined as follows. The probability of a sheet of electrons *not* being emitted within a time $t_j = j\delta t$ since the last emission is given by Eq. (30) as influenced by Eq. (28). Observe that this constitutes a separate requirement on the emission process distinct from, albeit related to, that behind the second model (M2). The algorithm computes the probability of an event at the cathode and samples a random number from a uniform distribution to check for the event (an "acceptance / rejection" algorithm). If an event occurs, a sheet of charge is created at the cathode ($z = 0$) carrying a charge density of $\sigma = J_{FN}(F)\Delta t_j$, where $\Delta t_j = j\delta t$ is the time between this emission and the previous emission. Observe that on average, $\langle \Delta t_j \rangle = \Delta t$. Then the time step is advanced and the process is repeated for a specified amount of time. For the initial emission at time $t = 0$, a value of $\Delta t_j = \tau_0/100$, where τ_0 is the characteristic transit time, is chosen. If no sheet of charge is emitted, the time step is advanced without the creation of any sheet charges.

The code keeps track of several different quantities: the distribution of emission times and transit times, the field and current density at the surface, the charge collected at the anode, and the sheet's trajectories as a function of time. The transit time of the individual sheets in the MC code can be tracked and compared to the ballistic transit time. Not surprisingly, the actual transit times are larger but the nature of the spread in transit times is as shown in Figure 7. As a result of the spread, and given the AK gap separation distance, occasions occur when one sheet can potentially overtake another; such instances do not occur in models M1 and M2. Although infrequent, overtaking events are observed in M3.

The results of the MC simulation for the $s - \tau$ approximation are shown in Figure 8, where the ratio of the current density to its initial value, along with the ratio of the surface field to V_a/D, is shown as a function of time as measured in units of the ballistic transit time. Compare the findings to those shown in Figures 5 and 6. The MC algorithm using the $s - \tau$ approximation is most closely similar to M2 but the finite time step δt and the form of the attempt probability $R(F)$ combine to affect how the oscillations unfold, most importantly in that the time to the next emission event cannot be arbitrarily small as Eq. (23) would allow (occurring when r_i is arbitrarily close to 1). This can be seen in a histogram of the values Δt_j takes in a typical simulation as shown in Figure 11. In contrast to the behavior of Figure 2, the short time Δt_j's are being suppressed in the MC simulation, due to

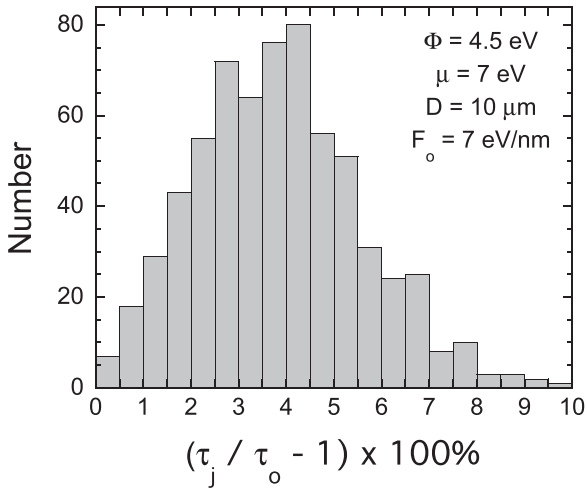

FIG. 7. Histogram of transit times τ compared to the ballistic transit time $\tau_o = \sqrt{2mD/F_o}$ and expressed as a percentage above τ_o in the $s - \tau$ approximation. The size of the bins is 0.5. A similar histogram is obtained when the position dependence of the sheets as per Eq. (19) is included.

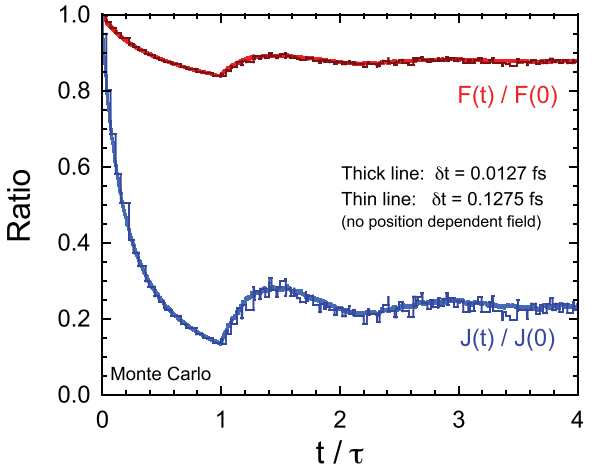

FIG. 8. Monte Carlo simulations using the $s-\tau$ approximation of the field emission planar diode for time steps $\delta t = 0.0127$ fs (short) and 0.1275 fs (long), where the emission probability is related to the number of electrons emitted per attempt (Eq. (28)).

the manner in which $R(F)$ in Eq. (2) affects the probability of the next emission event. A reduction of the short time events in number has the effect of dampening fluctuations and oscillations in $J(t)/J(0)$ as the sheets of charge are spread out more than would be if Δt_j were governed by Eq. (23) alone. Observe that such histograms depend only on the magnitude of the surface field, and it is therefore unsurprising that the $s-\tau$ approximation gives comparable results to when the position dependence of Eq. (19) is kept.

The results of the MC simulation for when the $s-\tau$ approximation is *not* made are shown in Figure 9, where the consequences of including the position dependence of the sheet of charges in Eq. (19) is evident in the transition from a staircase-like profile to a sawtooth-like shape: the j^{th} sheet is pushed towards the cathode by the sheets ahead of it, pushed towards the anode by the sheets behind it, and the force components of all the sheets are dependent upon their position in the AK gap. By comparison to the $s-\tau$ model, the simulation is consequently much more intensive. Observe that qualitatively the figure is quite similar to Figure

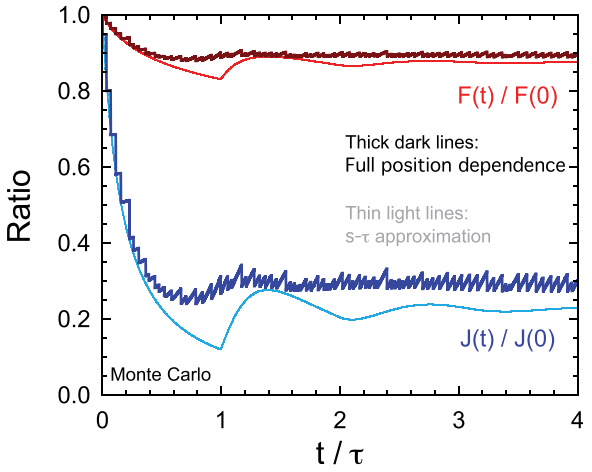

FIG. 9. Monte Carlo simulations accounting for the sheet position dependence of the field reduction at the surface compared to the M1 results (compare with Fig. 1 of Ref. 44).

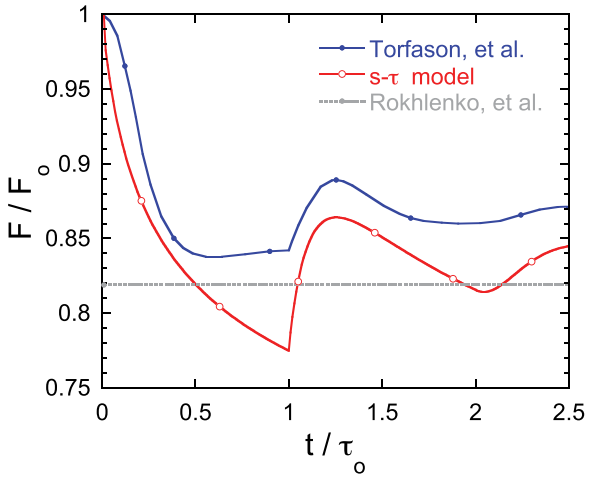

FIG. 10. The molecular dynamics simulations of Torfason *et al.* (data obtained from Figure 4 for $L = 2.5\,\mu$m and $D = 1\,\mu$m, with $\Phi = 2.0$ eV, $F = 2$ eV/nm) compared to the M1 $s-\tau$ simulation. See text for discussion. Observe the similarity of the MD results to the position-dependent M3 results of Figure 9.

1 of the analytical treatment of Rokhlenko and Lebowitz.[44] Specifically, the weakening of a sheet's ability to reduce the surface field as it approaches the anode as a consequence of the $(D-x)/D$ factor in Eq. (17) changes the injection of charge into the gap and tends to smooth out (larger) oscillations that otherwise occur if the influence of the leading sheets, which have the largest σ, are not attenuated as Eq. (17) prescribes. Importantly, such a position dependence is additionally evident in MD simulations that do not use a sheet-charge model: compare the results of the predictions of the position-dependent M3 simulation to the MD simulations of Torfason *et al.*,[26] as reproduced in Figure 10. In that work, the field was held at a lower value ($F = 2$ eV/nm) for a lower work function $\Phi = 2$ eV). In contrast to the planar model using sheets herein, the MD simulations launched individual electrons from a cathode region of finite extent:

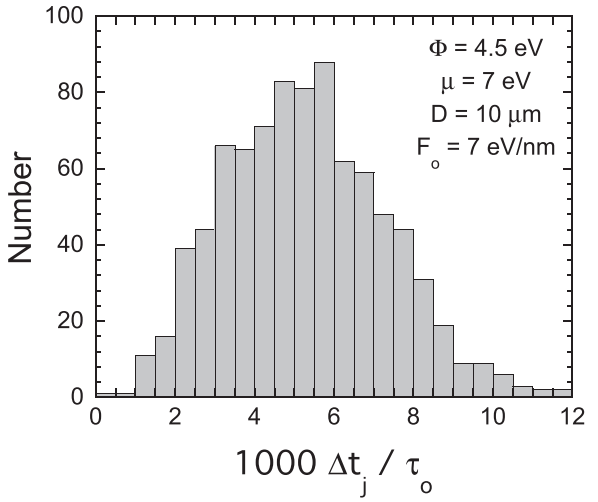

FIG. 11. Histogram of the next emission event Δt_j. Size of the bin is 0.5. Observe that in the larger bins, the counts appear to decline exponentially, but in the smaller bins, the counts decline as well. A similar histogram is obtained when the position dependence of the sheets as per Eq. (19) is included.

the square emitting area had a length of $L = 2.5\,\mu$m, and the anode-cathode separation was $D = 1\,\mu$m. The beam cross-section was therefore allowed to expand under space charge forces. Nevertheless, the MD simulations show the same basic relation to the M1 results that the position-dependent M3 results do.

A critical feature of the MC algorithm is the ability to chose the charge density of the sheets of charge that can be emitted per time step. In the hemispherical model (considered in Section IV), a constraint on this is in place due to the discrete nature of the electron charge.

IV. DISCRETE EMISSION FROM A HEMISPHERE

The simplest modification to the planar model is a hemisphere on plane model. It can be generalized to multiple protrusions, and provides a simple image charge approximation, but the field lines, and therefore transit times must be calculated numerically or obtained approximately.[18] The hemisphere is a limiting case of a prolate spheroidal geometry which analytically provides field lines, but multiple protrusions require the introduction of a Line Charge Model (LCM) and will therefore be considered in a separate work.[10,11]

The introduction of protrusions results in a range of transit times, non-uniform emission patterns, and image charge contributions that change with distance. In the case of a hemisphere, the influence of the image charge changes with distance depending on the size of the hemisphere, many image charges are present of which a subset dominate, and for rotationally symmetric structures the image charges are in the shape of rings of charge rather than point charges for the evaluation of the apex current density.

Geometric features on the surface gives rise to field enhancement factors (alternately called the "magnification" factors) that, as Kosmahl[46] argued are "*(t)o a good approximation. proportional to the height. and inversely proportional to the radius of the tip* in conical structures with rotational symmetry." (*emphasis in original*.) An assembly of protrusions can be modeled from single protrusion solutions using superposition, although nearby protrusions introduce a shielding effect that affects the putative apex radius and the shape of protrusions modeled from charge distributions in the Point and Line Charge Models. In contrast, physical field emitters do not change shape due to adjacent tips. Conditions at the apex matter most whereas the exact shape of boundaries further away become less consequential: for the same tip radius and apex field, the current from a protrusion only weakly depends on the shape of the body of the emitter, and then mostly through the behavior of the notional area factor $g(F)$ (Eq. (34)). For example, $g(F)$ for a hemisphere is $1/(b-\nu+4)$ compared to $1/(b-\nu+1)$ for an ellipsoid:[45] for $F = 5$ eV/nm and $\Phi = 4.5$ eV (giving $b = 13.04$ and $\nu = 0.7728$), the ellipsoid notional area is 82% that of the hemisphere.

A. Potential, field, and current

Using notations and methods of a previous treatment on emittance and surface roughness,[18] the potential $V(x)$ for a hemisphere on a flat plane immersed in a background field F_o is

$$V(r,\theta) = V_o - F_o r\cos\theta\left[1-\left(\frac{a}{r}\right)^3\right], \tag{32}$$

where θ is the polar angle, and $V_o = 0$ if the cathode is grounded (or $V_o = \mu + \Phi$ as for the emission equations where the bottom of the conduction band is the zero energy). Along the surface of the hemisphere ($r = a$), the field is normal to the surface and given by $F(a,\theta) = 3F_o\cos\theta$. The field enhancement is therefore $\beta(\theta) \equiv F/F_o = 3\cos\theta$. Although $\beta(\theta)$ varies over the surface of the emitter, conditions *at the apex* matter most: therefore the convention here is that β without an argument refers to the apex value, or $\beta(\theta) = \beta\cos\theta$, with $\beta = 3$ and $F_{tip} = \beta F_o$ for a hemisphere. Total current I is obtained by integrating the current density J over the surface Ω, accounting for geometry and field variation.[45] Total current I_{boss} is evaluated by

$$I_{boss} = \int_\Omega J(F(\Omega))d\Omega \approx 2\pi a^2 g(F_{tip})J(F_{tip}), \tag{33}$$

where Ω specifies the surface. For a hemisphere, using Eq. (A4) for $J(F)$ gives[18]

$$g(F) = \frac{1}{b}\int_0^\infty \left(1+\frac{x}{b}\right)^{\nu-4} e^{-x}dx \approx \frac{1}{b-\nu+4}, \tag{34}$$

where $x = b(\sec\theta - 1)$ and $b \equiv B\Phi^{3/2}/F$ is typically large, and $2\pi a^2 g(F)$ being the notional emission area which measures (but is smaller than) the fraction of the hemispherical surface that is emitting: for $\Phi = 4.5$ eV, $g(F) = F/(65.207 + 3.2272F)$ for F in [eV/nm].

The integrated current fraction $\Delta(\theta)$ is defined by[18] $\Delta(\theta) = I(\theta)/I_{boss}$, with $\Delta(\pi/2) = 1$, where θ replaces the upper limit of integration in Eq. (33) when $d\Omega = 2\pi a^2 \sin\theta d\theta$, or equivalently, the upper limit in Eq. (34) is replaced with $x_{max} = b(\sec\theta - 1)$. The current emitted from a ribbon of width $ad\theta$ between the angles θ_a and θ_b is therefore

$$dI(\theta) = I_{boss}(\Delta(\theta_b) - \Delta(\theta_a)). \tag{35}$$

B. Ring image charge

The image charge approximation to finding the potential of a charged particle outside a conducting sphere[32] is the basis for the ring model introduced now and the prolate spheroidal model to be introduced separately.[11] A charge outside a conducting sphere embedded in a flat plane with a close anode, shown in Figure 12, matches boundary conditions by the placement of image charges, the first of which is determined by considering the sphere in isolation. At a point $\vec{r}$, the potential due to a charge $-q$ and its image $q_i \equiv \kappa q$ is given by $V(\vec{r}) = 4Q(r_2^{-1} - \kappa r_1^{-1})$ where $4Q = q^2/4\pi\varepsilon_0$. Demanding that $V(a,\theta) = 0$ requires

$$\frac{4Q}{P(1-\gamma\cos\theta)^{1/2}} = \frac{4\kappa Q}{P'(1-\gamma'\cos\theta)^{1/2}}, \tag{36}$$

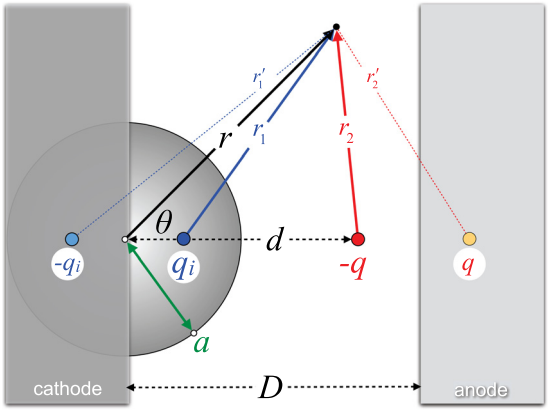

FIG. 12. Hemisphere on a flat surface. Anode is a distance D. Dominant image charges are shown for an external electron $-q$ (red). For $D \gg d \gtrsim a$, the image charge within the hemisphere dominates all others.

where $\gamma \equiv 2ad/P^2$ and $\gamma' \equiv 2ad'/P'^2$ with $P \equiv \sqrt{a^2+d^2}$ and $P' \equiv \sqrt{a^2+d'^2}$, where d' is the distance from the center of the sphere to the image charge q_i. Equation (36) is satisfied when $1/P = \kappa/P'$ and $\gamma = \gamma'$, which requires $d' = a^2/d$ and $\kappa = a/d$. The cathode and anode planes contribute planar image charges to maintain boundary conditions, and those image charges create others *ad infinitum*, but for a charge q just outside the sphere, and for D large compared to a, the four charges shown in Figure 12 dominate.

The influence of the image charge q' on the emitted electron $-q$ is given by $4\kappa Q/P'(1-\gamma')$ for on-axis dominated emission, or

$$V_{image}(r) = \frac{2Qa}{r^2 - a^2}, \tag{37}$$

for which, when $r = a + x$, gives $Q/x[1 + (x/2a)]$ which asymptotically approaches the standard planar image charge potential Q/x when $x/a \to 0$.

Emission from the hemisphere is rotationally symmetric, and can be represented as a sum over rings of charge, one of which is shown in Figure 13. If the edge of the ring is a distance R from the center of the hemisphere, and a distance r from the apex of the hemisphere, then the plane of the ring is a distance $R\cos\theta - a$ above the apex of the hemisphere. The field due to that ring is evaluated by letting the charge per unit length of the ring be $\sigma = \lambda q/2\pi R\sin\theta$, where λq is the

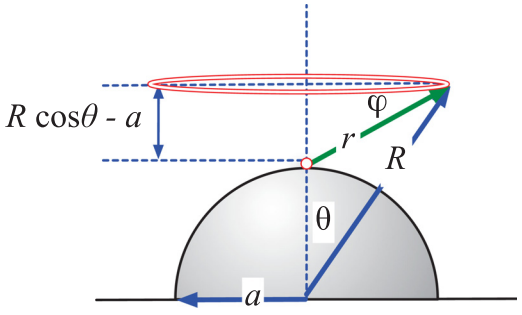

FIG. 13. Ring of charge and associated parameters to determine the apex field. θ is the polar angle and φ is the angle between r and the plane of the ring.

total charge on the ring. A small segment of the ring $ad\phi$ therefore contributes a factor $dF_z = q\sigma R\sin\theta d\phi\sin\varphi/r^2$ to the field at the apex of the hemisphere, where ϕ describes rotations about the axis of symmetry. The sum of the fields due to all of the elements of the ring produces a total field in the $\hat{z}-$ direction only given by

$$F_z = -\frac{4\lambda Q(R\cos\theta - a)}{[R^2 + a^2 - 2aR\cos\theta]^{3/2}}, \tag{38}$$

with the sign indicating the field is down (into the hemisphere). Because each charge element of the ring can make use of the analysis behind Eq. (36), it follows that the image charge ring in the hemisphere F'_z is given by

$$F'_z = -\left(\frac{R}{a}\right)\frac{4\lambda Q(R - a\cos\theta)}{[R^2 + a^2 - 2aR\cos\theta]^{3/2}}. \tag{39}$$

The total field due to the rings is then the sum of Eqs. (38) and (39): it is

$$F_z + F'_z = -\frac{4\lambda Q(R^2 - a^2)}{a(R^2 + a^2 - 2Ra\cos\theta)^{3/2}}. \tag{40}$$

Here, the parameter λ is the number of electrons contained in the ring. A single ring at a distance $R = 3a$ from the center of the hemisphere of radius $a = 5$ nm such that $\theta = \pi/4$, as in Figure 13, will suppress a background field of $F_o = 3$ eV/nm (that is, drive the apex field to 0) if $\lambda = 270$. Under conditions of actual emission, however, multiple rings will correspond to an emission "event." Each of the rings have their height and radius change as a consequence of their motion as the electrons in a ring move along their trajectory arcs. Therefore, to use the ring model to investigate space charge, the charge for each ring λ_j and the time dependent radius $\rho(t)$ and height $z(t)$ of each ring must be found,.

There are two approaches for specifying the charge λ_j in a ring. The first uses the integrand of Eq. (34). The initial conditions of the ring $(\rho_j(0), z_j(0))$ are specified by the middle of the ribbon strip defining the differential emission element. Passing over to a summation rather than integration, $g(F) = \int dg \to g(F)\sum_{j=1}^{N} f_j$ where θ_j is discretized to N locations to characterize N rings according to

$$\theta_j \equiv \frac{(2j-1)\pi}{4N} \equiv \left(j - \frac{1}{2}\right)\Delta\theta, \tag{41}$$

so that $\theta_{1/2} = 0$ and $\theta_{N+1/2} = \pi/2$. For a ribbon of center radius $a\sin\theta_j$ and width $a\Delta\theta$, the fraction f_j of the total emitted charge contained in the ribbon is approximated by

$$f_j \approx \frac{\exp(-\phi_{j-1/2}) - \exp(-\phi_{j+1/2})}{g(F)}, \tag{42}$$

where $\phi_x = (\sec\theta_x - 1)/(b - \nu + 4)$. Therefore, this method requires bookkeeping of the ring charges, as would be required to estimate the impact of space charge on emittance in the surface roughness model.

The second approach is to make use of the notional area approximation of Ref. 45 and is motivated by the observation

that along the $\hat{z}-$axis, $V(z)$ for a ring with charge λq, of radius ρ, and a distance z away, is $V_{ring}(z) = \lambda Q/R$, where $R^2 = \rho^2 + z^2$: that is, it is equivalent to a point charge a distance R away where R is the distance to any element of the ring. The approximation simplifies the analysis for rings originating from a hemisphere such that their positions do not depart significantly from a hemispherical shape during their transit. As the current from a hemisphere depends on the product of an area factor with apex current density, where the former varies weakly and the later strongly with field, the approximation is reasonable and enables a formulation more amenable to analysis. The notional angle is then given by (Eq. (26) of Ref. 45)

$$\cos\theta_n = 1 - \int_0^{\pi/2} \sin\theta \frac{J(F(\theta))}{J(F(0))} d\theta, \tag{43}$$

$$\approx \frac{b+3-\nu}{b+4-\nu}, \tag{44}$$

where the "n" subscript refers to "notional" angle. It is convenient to introduce $\eta \equiv \cos\theta_n$. Even though the current density on axis is largest, the charge associated with its ring is affected by the emission area ribbon, and so the charge on the $j-q$ ring peaks near $\cos\theta_j \approx \eta$, as shown in Figure 14, an observation with consequences for the emittance associated with a field emitter as pointed out by Whaley (see Figure 9 of Ref. 47). The notional approximation represents the cumulative effect of all the differential rings as one ring originating at $\theta = \theta_n$ with a number of electrons $\lambda = I_{boss}\Delta t/q$. The approximation is only appropriate as a simple model to quantify estimates of space charge effects that is convenient for analysis: it is not sufficient to address the impact of space charge on emittance in the surface roughness model.

C. Height, radius, and transit time

The transit time of an electron from the hemisphere to a planar anode a distance D away may be estimated using the impulse approximation.[45] In the absence of space charge, in a field of F_o with an initial velocity of $\sigma_i v_F \cos\theta$, where $v_F = \sqrt{2\mu/m}$ and σ_i is the magnitude of the impulse modification (the "i" subscript to distinguish it from the surface charge density σ factor), the motion is ballistic. The coordinates of the j^{th} ring of radius $\rho_j(t)$ and height $z_j(t)$ are therefore

$$z_j(t) = (a + \sigma_i v_F t)\cos\theta_j + \frac{F_o}{2m}t^2, \tag{45}$$

$$\rho_j(t) = (a + \sigma_i v_F t)\sin\theta_j, \tag{46}$$

and $R_i(t)$ (corresponding to R in Eq. (40)) is

$$R_j(t)^2 = z_j(t)^2 + \rho_j(t)^2. \tag{47}$$

The transit time τ_j of the j^{th} ring for an anode-cathode (AK) separation of D is therefore a solution of the quadratic equation

$$\frac{F_o}{2m}\tau_j^2 + (a + \sigma_i v_F \tau_j)\cos\theta_j - D = 0. \tag{48}$$

The approximation, developed in Ref. 45, for σ_i is

$$\sigma_i = \sqrt{1 + \frac{7F_o a}{2\hbar k_F}}, \tag{49}$$

where $\hbar k_F$ is the Fermi momentum. Electrons emitted at larger angles θ have smaller initial velocities in the $\hat{z}$-direction, and although all final energies of all electrons at the anode are the same, those emitted off-axis have a transverse velocity component $E_\perp = (1/2)m(\sigma_i v_F \sin\theta)^2$: the cumulative effect of both results in the transit time off-axis being larger than on, as shown in Figure 15 for $D = 10$ μm, for which the on-axis transit time is

$$\tau(0) = \frac{2D}{v_b}\left(\frac{\zeta(1-\delta)}{\sqrt{1+\zeta^2(1-\delta)}+1}\right), \tag{50}$$

where $\delta = a/D$ and $\zeta = v_b/v_o$ with $(1/2)mv_b^2 = F_o D$. For ζ large and δ negligible,

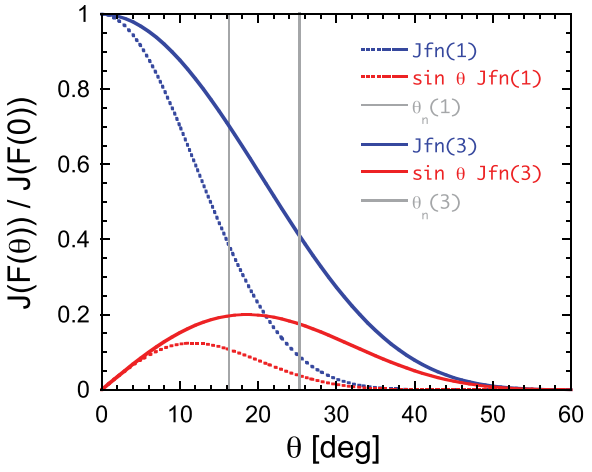

FIG. 14. The ratio $J(\theta)/J(0)$ and proportion of emitted current $\sin\theta J(\theta)/J(0)$ as a function of polar angle θ. $\theta_n(F)$ is the notional angle. Numbers in parentheses refer to F_o in units of eV/nm.

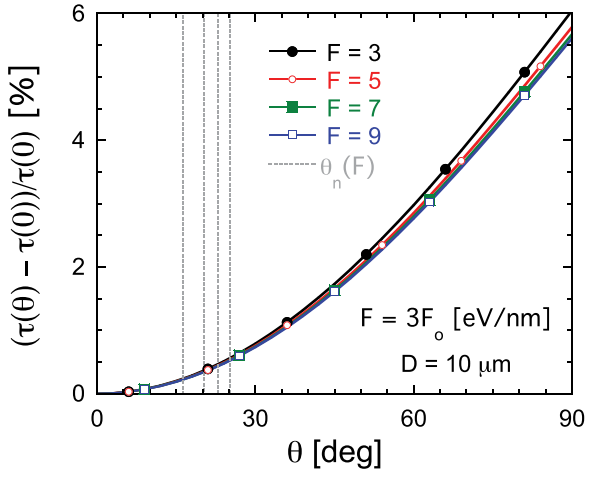

FIG. 15. Off-axis $\tau_j = \tau(\theta_j)$ compared to on-axis $\tau(0)$ transit times for $\mu = 7$ eV, $\Phi = 4.5$ eV, $a = 10$ nm, and $D = 10$ μm, in the impulse approximation. Grey dashed lines indicate the locations of the notional angle $\theta_n(F)$ for increasing F from left to right, defined in Eq. (43).

$$\frac{\tau(\theta)}{\tau(0)} \approx \frac{\sqrt{\zeta^2+1}+1}{\sqrt{\zeta^2+\cos^2\theta}+\cos\theta}. \tag{51}$$

For the conditions of Figure 15, $\zeta = 17.03$, 17.77, 18.12, and 18.32, for $3F_o = 3$, 5, 7, and 9 eV/nm, respectively. The on-axis transit time for the lowest field is $\tau(0) = 317.8$ fs, When D decreases for the same a (δ increases), the differences become more pronounced. Again for $F_o = 1$ eV/nm, then for $D = 1$ and 0.1 μm ($\delta = 0.01$ and 0.1), $\tau(0) = 88.14$ and 17.82 fs, and $\zeta = 5.39$ and 1.70, respectively, resulting in $100\%[(\tau(\pi/2)/\tau(0)) - 1] = 21\%$ and 89%, respectively, with the intermediate θ−dependence scaling very similar to that shown in Figure 15. Thus, micro- and nano-gaps are more susceptible to transit time induced effects resulting from off-axis parabolic trajectories than are gaps 10's of microns or more, even though field emission becomes negligible after $\theta \sim 50^\circ$ when $F_o = 3$ eV/nm (and smaller for lower fields). This conforms with intuition in that with respect to the transit time, as D increases, the influence of the velocity v_z increases over the duration of the transit (i.e., $v_z/v \to 1$), but the contribution of v_ρ is fixed by conditions near the hemisphere and its influence is therefore limited to distances comparable to the hemisphere radius, as assumed in the impulse approximation.

A consequence of the variation of transit time with launch angle is that the rings of charge will spread out during transport across the AK gap, so that the sharp changes in surface field suggested by the 1D sheet charge model will instead be softened: in the ring charge model, a natural damping is thereby introduced. To leading order, and using Eq. (51) and $F_oD = (1/2)m(\zeta v_o)^2$, the difference in arrival times of the largest possible ring ($\theta = \pi/2$) with the on-axis ring is

$$\tau(\pi/2) - \tau(0) \approx \frac{mv_o}{F_o}\left(1 - \frac{1}{2\zeta}\right), \tag{52}$$

and therefore, due to the general largeness of 2ζ, does not vary greatly as D is changed for a given F_o, even though $\tau(0)$ does. Because $\tau(\theta_n)$ scales with $\tau(\pi/2)$, as in Figure 15, the conclusion is that the usage of a single notional ring to represent all the rings does not run afoul of a distribution in arrival times of the numerous rings which it represents, particularly as the charge per ring for the rings with $\cos\theta_j \approx \eta$ dominate.

The decrement of the apex field on the hemisphere $\Delta F(t)$, therefore, is given by summing over all the rings as they move away from the hemisphere with their coordinates governed by Eqs. (45) and (46) or

$$\Delta F(t) = -\sum_{j=1}^{N} \frac{4\lambda_j Q}{aN} \frac{\rho_j(t)^2 + z_j(t)^2 - a^2}{\left[\rho_j(t)^2 + (z_j(t) - a)^2\right]^{3/2}}, \tag{53}$$

where λ_j is the charge carried by ring j. In the notional approximation, a single ring is launched at the notional angle θ_n with the entire emitted charge and the trajectory of that ring to be determined. For that single ring (compare Eq. (40))

$$\Delta F_n(t) = -\frac{4\lambda Q}{a} \frac{\rho_n(t)^2 + z_n(t)^2 - a^2}{\left[\rho_n(t)^2 + (z_n(t) - a)^2\right]^{3/2}}, \tag{54}$$

where $\theta_j \to \theta_n$ in the definition of ρ and z (the subscript "n" denotes "notional" and not an index). The notional trajectories are shown in Figure 16 for representative background fields.

D. Unit cell space charge

Field emission along the hemisphere will be strongly suppressed until such time as the notional ring moves far enough away that the field at the apex can rebound. The time to do so is a field-dependent characteristic time. The dependence of space charge on surface field, which in turn depends on the nature of surface roughness, thereby introduces an increased sensitivity to space charge compared to the 1D models (although the field reduction at the surface of the cathode due to a sheet of charge being dependent on the sheet's distance has an analog in that a ring of charge approaching the anode generates an image ring beyond the anode plane, and so the influence of the ring weakens further as it approaches the anode). When roughness is present, the background field F_o is lower, in the case of a hemisphere, by a factor of 3 compared to fields assumed in the 1D models. In turn, the ballistic transit time will be larger by the same factor, and therefore the time that charge is in the AK gap increases. Therefore, an understanding of space charge forces is more involved than in the 1D analyses, even though at a distance of several hemisphere radii from the surface (smaller when the pitch of the hemispheres is greater), the equipotential lines flatten.

This suggests that a "unit cell" can be demarcated such that within it, notional rings of radius $\rho(t)$ follow trajectories dictated by Eqs. (45) and (46) with θ_j replaced by the notional angle θ_n. Once $z(t)$ crosses the "virtual anode" of the unit cell,[45] the 1D description for sheets of charge resumes, with the charge density per sheet given by $I_{boss}\Delta t/d_{tt}^2$. The dimensions of the cell can be determined in

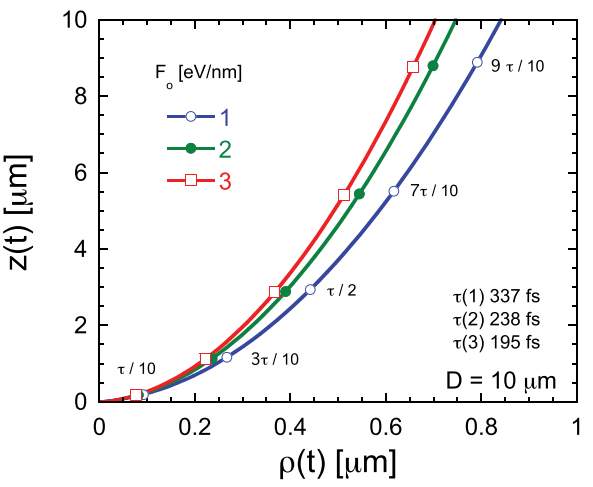

FIG. 16. Notional ring trajectories for background fields of 1 eV/nm (blue open circle), 2 eV/nm (green closed circle), and 3 eV/nm (red open square). The labeled points are fractions of a ballistic transit time $\tau_o = \sqrt{2mD/F_o}$.

two ways. The first, which will be used below, is to set the "virtual anode" at the location where $\Delta F_n(t)$ of Eq. (54) ceases to appreciably affect emission. The second, which will be used in follow-on studies for the understanding of shielding effects,[11] sets the virtual anode at a location comparable to the pitch, or tip-to-tip separation, of the hemispheres or emission sites (if wires or ellipsoids), where the cumulative interaction of all the emitters is such that the equipotential lines flatten to a degree that renders the approximation appropriate. Observe that either method will identify when space charge effects within the unit cell become important, but not what the self-consistent space charge limited flow is, which requires the coupling of trajectory-based unit cell models with particle-in-cell simulations (and is under development). Therefore, for purposes of the unit cell study, D will refer to the distance to the virtual anode in the unit cell, and the boss will be treated as if there were no others.

Emission is space charge affected when the current I_{boss} of Eq. (33) becomes a fraction ϵ of what it would be were $F_{tip} = 3F_o$ not reduced, that is

$$\epsilon \equiv \frac{I_{boss}(3F_o - \Delta F_n)}{I_{boss}(3F_o)} \approx \exp\left(-\frac{(b_o + 3 - \nu)}{3F_o}\Delta F_n\right), \tag{55}$$

where $b_o = B\Phi^{3/2}/3F_o$, and assuming that for room temperature conditions, field emission current density can be modeled using J_{FN}. Note that ϵ is not necessarily small. Use Eq. (54) to introduce the function $U(s)$ defined by $\Delta F_n(s\tau) \equiv -(4\lambda Q/a)U(s)$, where $s = t/\tau$. This equation holds for but one ring, but when more than one ring is present, all the notional rings must be summed to find the field reduction at the surface. Let $n = \lfloor \tau/\Delta t \rfloor$ where $\lfloor \cdots \rfloor$ is the round down integer operation. For the values of $\mu = 7$ eV, $a = 50$ nm, and $\lambda = 1$, $n = 22$, 267, 675, and 1476 for F_o [eV/nm] = 2, 2.5, 2.75, and 3.0, respectively. Thus, even the value of the first term of the series $U(1/n)$ varies markedly, as suggested in Figure 17. Then, and as shown in Figure 18,

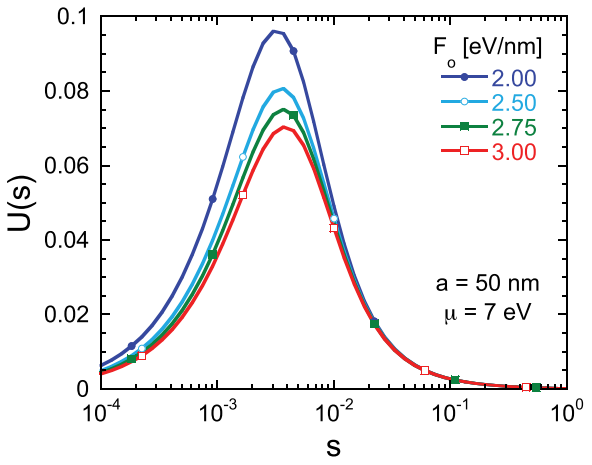

FIG. 17. The function $U(s) = -a\Delta F_n(s\tau)/4\lambda Q$ using Eq. (54) for $a = 50$ nm, $\mu = 7$ eV, $D = 10\,\mu$m, $\lambda = 1$, and $n = \lfloor \tau/\Delta t \rfloor$.

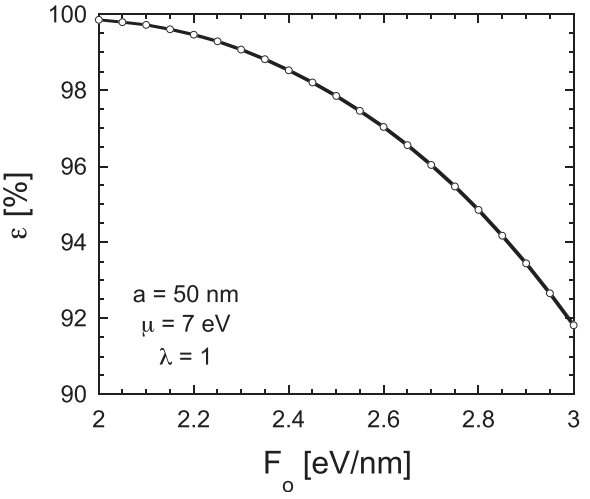

FIG. 18. The reduction in current from a single hemispherical boss for various fields expressed as a percentage reduction (Eq. (56)), using the parameters of Figure 17.

$$-\ln(\epsilon) \approx \frac{4\lambda Q}{3aF_o}(b_o + 3 - \nu)\sum_{j=1}^{n} U\left(\frac{j}{n}\right). \tag{56}$$

A second requirement is that λ be reasonable: it should not correspond to an unphysical fraction of an electron charge, but neither should it represent so much charge that the emitted ring undergoes strong internal space charge forces at the outset: that is, λ should be a parameter of order unity.

The onset of SCAFE may therefore be monitored by the behavior of ϵ as a function of F_o. The behavior is shown in Figure 17. In a diode configuration with surface roughness at the cathode, a hemispherical bump would not exist in isolation as the model treated here presumes, but rather there would be many such bumps, and therefore the unit cell AK gap to the virtual cathode would have to be comparable to the representative bump-to-bump separation d_{tt} because of the effects of shielding. Such a model treats surface roughness as more nuisance than desideratum in characterizing the influence of roughness on the current that can be drawn across a diode configuration. When field emission is desired, the emitters are more conical[48,49] or wire-like.[9,50] Shielding is therefore dependent on the character of the emitter itself and shall be taken up separately.[11]

V. SUMMARY

Space charge affected field emission conditions in a diode geometry have been considered from the perspective of discrete emission events. In the purely one-dimensional model, sheets of charge are randomly emitted, and oscillations in the current density are seen to arise as a consequence of the transit time of the first sheet across the AK ap. When a model of surface roughness is introduced, the flexibility in choosing the charge density of the sheets is further constrained by the emission from a protrusion. The cross-over between the one dimensional model and the three dimensional surface roughness model is determined by the mean distance between surface roughness features due to how the protrusions shield each other. The unit cell containing a single emitting feature is dictated by the protrusion-to-protrusion

separation. Within the unit cell, space charge reduction of the apex field was modeled by the emission of a notional ring of charge plus its image charge in the hemispherical model. An estimate of the field reduction at the apex, and its associated current per protrusion reduction, was given. The amount of charge in the emitted ring is constrained by the discrete nature of electron charge, in distinction to the one dimensional diode model. The components of the model are directed to provide a means of introducing the effects of surface roughness and its related field enhancement into beam optics codes (aka particle-in-cell or PIC codes) as well as more conventional conical emitters or, in particular, field emission from elongated carbon fibers with a mean separation smaller than their length.

ACKNOWLEDGMENTS

We gratefully acknowledge financial support from J. Luginsland and J. Marshall (AFOSR). This research was performed while IMR held a National Research Council Research Associateship Award at the Naval Research Laboratory.

APPENDIX A: THERMAL-FIELD EQUATION

The general Thermal-Field (GTF) equation is[18]

$$J(F,T) = A_{RLD}T^2 N\left[\frac{\beta_T}{\beta_F}, \beta_F(E_o-\mu)\right], \tag{A1}$$

$$N(n,s) \approx n^2\Sigma\left(\frac{1}{n}\right)e^{-s} + \Sigma(n)e^{-ns}, \tag{A2}$$

where $\beta_T = 1/k_BT$, $\beta_F = \partial_E\theta(E)$, where $\theta(E)$ is the Gamow factor associated with tunneling, and $\Sigma(x) \approx (1+x^2)/(1-x^2)\ -0.355x^2(1+0.298x^2)$ to leading order.[18] For the GTF equation, n is the ratio of the energy slope factors, or $n \equiv \beta_T/\beta_F$. For $n \to 0$, the Richardson-Laue-Dushman equation results

$$J_{RLD}(F,T) = A_{RLD}T^2\exp\left(-\frac{\Phi-\sqrt{4QF}}{k_BT}\right), \tag{A3}$$

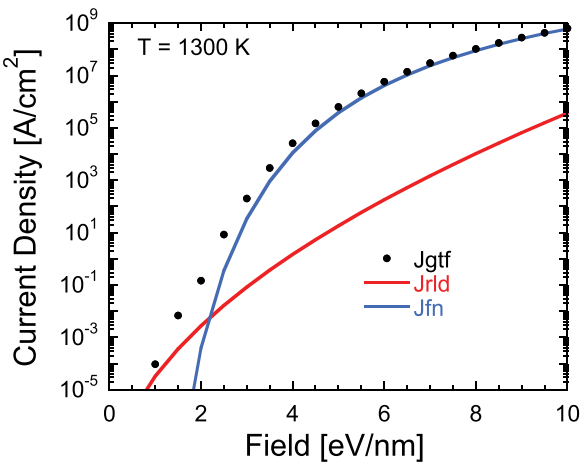

FIG. 19. Comparison of the general thermal field current density J_{GTF} of Eq. (A1) with the Fowler Nordheim (field) current density J_{FN} of Eq. (A4) and the Richardson (thermal) current density J_{RLD} of Eq. (A3) for a temperature of 1300 K for $\Phi = 4.5$ eV and $\mu = 7$ eV.

where $\sqrt{4QF}$ accounts for Schottky barrier lowering due to the field F. For $1/n \to 0$, the Fowler Nordheim equation results and $\theta(E)$ is given by conventional Fowler-Nordheim theory. Using the Deane and Forbes[51] approximation $v(y) = 1 - \frac{1}{3}y^2(3-\ln(y))$ and letting $t(y) = t_o \equiv 1+(1/6e) = 1.0613$, then

$$J_{FN}(F) = \tilde{A}F^{2-\nu}\exp\left(-B\frac{\Phi^{3/2}}{F}\right), \tag{A4}$$

where $\nu \equiv (8Q/9\hbar)\sqrt{2m/\Phi}$, $\tilde{A} \equiv (A/\Phi t_o^2)(\Phi^2e^6/4Q)^\nu$, $t_o^2 \approx 1.1264$, $A = q/(16\pi^2\hbar) = 1.5414\times10^{-6}$ Amp/eV, $B = 4\sqrt{2m}/3\hbar = 6.8309$ 1/nm-eV$^{1/2}$, and $Q \equiv q^2/16\pi\varepsilon_o = 0.35999$ eV-nm. For $\Phi = 4.5$ eV, $\nu = 0.77281$. A comparison of J_{GTF} to J_{RLD} and J_{FN} is shown in Figure 19. It is emphasized that the Nordheim functions $v(y)$ and $t(y)$ are *implicitly* contained in the factors ν and t_o.

APPENDIX B: CHILD-LANGMUIR EQUATION

For $V_a = q\varphi_a$, the Child-Langmuir equation is

$$J_{CL}(V_a,D) = \frac{q}{18\pi Q\sqrt{2m}}\frac{V_a^{3/2}}{D^2} = \frac{4\varepsilon_0}{9}\sqrt{\frac{2q}{m}}\frac{\varphi_a^{3/2}}{D^2}, \tag{B1}$$

where φ_a is the anode potential and D is the anode-cathode (AK) separation, and where the form using φ_a is the more conventional form encountered. If written as $J_{CL} = KV_a^{3/2}$, where K is the analog of perveance, then for $D = 10\,\mu$m, $K = 2.334$ Amp / (eV $^{3/2}$ cm^2).

APPENDIX C: GENERATION OF RANDOM EMISSION EVENTS

Methods to generate random numbers of various distributions are known.[52] A probability of occurrence $P(x)dx$ (an "event") for a given distribution $P(x)$ is desired to be evaluated from the generation of a uniform random number r such that $0 \le r \le 1$. An acceptance/rejection approach is a common technique but can become computationally burdensome if $P(x)$ is small for a range of values. Some forms of $P(x)$ enable alternate approaches. The two treated here are linear and exponential. Observe that $P(x)$ satisfies

$$\int_0^L P(x)dx = 1, \tag{C1}$$

where L is the range of x over which the distribution $P(x)$ is non-zero (L can be infinite). The integration can be separated into regions that contain the same number of events when the total number of events is large. That is, if there are n such regions, then for $j = 0, 1, \ldots n-1$,

$$\int_{x_j}^{x_{j+1}} P(x)dx = 1/n. \tag{C2}$$

Two cases are of interest in the present study: (*i*) $P(x)$ is linear, and (*ii*) $P(x)$ is exponential.

In the linear case with $L=1$, then $P(x)=2x$. Thus, the x_j are determined by the relationship $x_j^2 - x_{j-1}^2 = 1/n$, or

$$x_j = \left(\frac{j}{n}\right)^{1/2}. \tag{C3}$$

In the limit that $n \to \infty$, $(j/n) \to r$, and so a random number x that is linearly distributed can be generated from a uniformly distributed r by $x(r)=\sqrt{r}$.

In the exponential case, $L \to \infty$ and $P(x)=e^{-x}$ (λ is taken as 1), from which $\exp(-x_{j-1}) - \exp(-x_j) = 1/n$, or

$$x_j = -\ln\left(1 - \frac{j}{n}\right). \tag{C4}$$

Again, letting $(j/n) \to r$ identifies $x(r) = -\ln(1-r)$, but because r is uniformly distributed, so is $1-r$, and so $x(r) = -\ln(r)$, from which Eq. (23) is obtained. This result corresponds to the $m=0$ (no "occurrences") special case of an algorithm described by Knuth (Ref. 53, p. 132) for the treatment of Poisson distributions, from which the designation "K" in Figure 2 originates.

An alternate method to generate an exponential-like distribution for N events is to create n bins governed by Eq. (C4), each containing (N/n) counts per bin (such an approach is reminiscent of methods to circumvent the computational burden of low probability events by grouping them into classes from which selections are made[54]). If n is reasonably large, then inside each bin, the distribution of random events can be taken as linearly distributed. Thus, the exponential distribution can be mimicked by generating two random numbers: r_1 chooses the j^{th} bin according to $j-1 = \lfloor nr_1 \rfloor$, and r_2 specifies the location x in the bin according to $(x_{j+1}-x)/(x_{j+1}-x_j) = \sqrt{r_2}$. This method was labeled "IMC" in Figure 2. It is less efficient than Eq. (C4) but performs better on the exponential distribution for large x than would a standard acceptance/rejection algorithm, and an understanding of it is conceptually useful in approaching the notional ring model.

[1]J. P. Barbour, W. Dolan, J. Trolan, E. Martin, and W. Dyke, Phys. Rev. **92**, 45 (1953).
[2]A. E. Bell and L. W. Swanson, Phys. Rev. B **19**, 3353 (1979).
[3]Y. Lau, Y. Liu, and R. Parker, Phys. Plasmas **1**, 2082 (1994).
[4]K. L. Jensen, M. Kodis, R. Murphy, and E. G. Zaidman, J. Appl. Phys. **82**, 845 (1997).
[5]R. Murphy and M. Kodis, *Vacuum Microelectronics* (Wiley, New York, 2001), p. 349.
[6]J. Luginsland, Y. Lau, R. Umstattd, and J. Watrous, Phys. Plasmas **9**, 2371 (2002).
[7]G. Chen, W. Wang, J. Peng, C. He, S. Deng, N. Xu, and Z. Li, Phys. Rev. B **76**, 195412 (2007).
[8]R. G. Forbes, J. Appl. Phys. **111**, 096102 (2012).
[9]W. Tang, D. Shiffler, K. Golby, M. LaCour, and T. Knowles, J. Vac. Sci. Technol. B **30**, 061803 (2012).
[10]J. R. Harris, K. L. Jensen, D. A. Shiffler, and J. J. Petillo, "Shielding in Ungated Field Emitter Arrays" (submitted).
[11]K. L. Jensen, D. A. Shiffler, J. R. Harris, J. J. Petillo, I. Rittersdorf, W. Tang, J. L. Lebowitz, Y. Y. Lau, and J. W. Luginsland, "Discrete space charge affected field emission: Conical and Wire Emitters" (unpublished).
[12]D. A. Shiffler, W. Tang, K. L. Jensen, J. R. Harris, J. J. Petillo, I. Rittersdorf, J. L. Lebowitz, Y. Y. Lau, and J. W. Luginsland, "Effective Field Enhancement Factor and the Influence of Emitted Space Charge" (submitted).
[13]Y. Lau, J. Appl. Phys. **62**, 351 (1987).
[14]A. Rokhlenko and J. Lebowitz, J. Appl. Phys. **102**, 123307 (2007).
[15]K. L. Jensen, J. J. Petillo, E. J. Montgomery, Z. Pan, D. W. Feldman, P. G. O'Shea, N. A. Moody, M. Cahay, J. E. Yater, and J. L. Shaw, J. Vac. Sci. Technol. B **26**, 831 (2008).
[16]J. Luginsland, M. Arman, and Y. Lau, Phys. Plasmas **4**, 4404 (1997).
[17]K. L. Jensen, J. L. Lebowitz, Y. Y. Lau, and J. W. Luginsland, J. Appl. Phys. **111**, 054917 (2012).
[18]K. L. Jensen, D. A. Shiffler, J. J. Petillo, Z. Pan, and J. W. Luginsland, Phys. Rev. ST Accel. Beams **17**, 043402 (2014).
[19]R. Forbes, J. Appl. Phys. **104**, 084303 (2008).
[20]Y. Feng and J. Verboncoeur, Phys. Plasmas **13**, 073105 (2006).
[21]A. Rokhlenko, K. L. Jensen, and J. L. Lebowitz, J. Appl. Phys. **107**, 014904 (2010).
[22]S. Sun and L. Ang, Phys. Plasmas **19**, 033107 (2012).
[23]A. Valfells, D. W. Feldman, M. Virgo, P. G. O'Shea, and Y. Y. Lau, "Effects of pulse-length and emitter area on virtual cathode formation in electron guns," Phys. Plasmas **9**(5), 2377 (2002).
[24]R. Umstattd, C. Carr, C. Frenzen, J. Luginsland, and Y. Lau, Am. J. Phys. **73**, 160 (2005).
[25]A. van der Ziel, *Solid State Physical Electronics* (Prentice-Hall, Englewood Cliffs, NJ, 1968), p. 156.
[26]K. Torfason, A. Valfells, and A. Manolescu, Phys. Plasmas **22**, 033109 (2015).
[27]L. K. Ang, T. J. T. Kwan, and Y. Y. Lau, Phys. Rev. Lett. **91**, 208303 (2003).
[28]L. K. Ang, W. S. Koh, Y. Y. Lau, and T. J. T. Kwan, Phys. Plasmas **13**, 056701 (2006).
[29]Equation (12) of Ref. 17 omitted a power of 2 from F in the denominator of the term $qJ/\varepsilon_o F^2$; it has been corrected here.
[30]R. Kishek and Y. Lau, Phys. Plasmas **3**, 1481 (1996).
[31]P. Christenson, D. Chernin, A. Garner, and Y. Lau, Phys. Plasmas **3**, 4455 (1996).
[32]L. Eyges, *The Classical Electromagnetic Field* (Addison-Wesley Publishing Company, Reading, Massachusetts, 1972).
[33]J. J. Petillo, E. Nelson, J. Deford, N. Dionne, and B. Levush, IEEE Trans. Electron Devices **52**, 742 (2005).
[34]R. E. Caflisch and M. S. Rosin, Phys. Rev. E **85**, 056408 (2012).
[35]R. G. Forbes and K. L. Jensen, Ultramicroscopy **89**, 17 (2001).
[36]Y. Zhu and L. Ang, Appl. Phys. Lett. **98**, 051502 (2011).
[37]C. K. Birdsall and W. B. Bridges, *Electron Dynamics of Diode Regions* (Academic Press, New York, 1966).
[38]R. B. Ash, *Basic Probability Theory* (Wiley, New York, 1970), pp. ix, 337.
[39]M. Cahay, K. L. Jensen, and P. von Allmen, in *Noise and Fluctuations Control in Electronic Devices*, edited by A. A. Balandin (American Scientific Publishers, Stevenson Ranch, California, 2002).
[40]K. Rangaswamy, M. Cahay, and K. L. Jensen, J. Vac. Sci. Technol. B **23**, 380 (2005).
[41]L. D. Smullin and H. A. Haus, *Noise in Electron Devices*, Technology Press Books in Science and Engineering (Published Jointly by the Technology Press of Massachusetts Institute of Technology and Wiley, Cambridge, New York, 1959), p. 413.
[42]C. A. Spindt, I. Brodie, L. Humphrey, and E. R. Westerberg, J. Appl. Phys. **47**, 5248 (1976).
[43]F. Read and N. Bowring, Nucl. Instrum. Methods Phys. Res. A **531**, 407 (2004).
[44]A. Rokhlenko and J. L. Lebowitz, J. Appl. Phys. **113**, 063304 (2013).
[45]K. L. Jensen, *Encyclopedia of Electrical and Electronics Engineering* (John Wiley & Sons, Inc., 2014).
[46]H. Kosmahl, IEEE Trans. Electron Devices **38**, 1534 (1991).
[47]D. R. Whaley, IEEE Trans. Electron Devices **61**, 1726 (2014).
[48]D. Whaley, B. Gannon, C. Smith, C. Armstrong, and C. Spindt, IEEE Trans. Plasma Sci. **28**, 727 (2000).
[49]P. R. Schwoebel, C. A. Spindt, and C. Holland, J. Vac. Sci. Technol. B **23**, 691 (2005).
[50]D. Shiffler, J. Luginsland, M. Ruebush, M. Lacour, K. Golby, K. Cartwright, M. Haworth, and T. Spencer, IEEE Trans. Plasma Sci. **32**, 1262 (2004).
[51]J. H. B. Deane and R. G. Forbes, J. Phys. A: Math. Theor. **41**, 395301 (2008).
[52]R. Y. Rubinstein, *Simulation and the Monte Carlo method*, Wiley Series in Probability and Mathematical Statistics (Wiley, New York, 1981).
[53]D. E. Knuth, *Seminumerical Algorithms*, Vol. 2 of The Art of Computer Programming (Addison-Wesley Pub. Co., Reading, Massachusetts, 1981).
[54]A. Bortz, M. Kalos, and J. Lebowitz, J. Comput. Phys. **17**, 10 (1975).